

UC Irvine

UC Irvine Previously Published Works

Title

Lipid remodeling in response to methionine stress in MDA-MBA-468 triple-negative breast cancer cells.

Permalink

<https://escholarship.org/uc/item/5df8z64q>

Authors

Borrego, Stacey L
Fahrmann, Johannes
Hou, Jue
et al.

Publication Date

2021

DOI

10.1016/j.jlr.2021.100056

Peer reviewed

Journal Pre-proof

Lipid remodeling in response to methionine stress in MDA-MBA-468 triple-negative breast cancer cells

Stacey L. Borrego, Johannes Fahrman, Jue Hou, Da-Wei Lin, Bruce J. Tromberg, Oliver Fiehn, Peter Kaiser

PII: S0022-2275(21)00038-9

DOI: <https://doi.org/10.1016/j.jlr.2021.100056>

Reference: JLR 100056

To appear in: *Journal of Lipid Research*

Received Date: 15 September 2020

Revised Date: 12 February 2021

Accepted Date: 19 February 2021

Please cite this article as: Borrego SL, Fahrman J, Hou J, Lin DW, Tromberg BJ, Fiehn O, Kaiser P, Lipid remodeling in response to methionine stress in MDA-MBA-468 triple-negative breast cancer cells, *Journal of Lipid Research* (2021), doi: <https://doi.org/10.1016/j.jlr.2021.100056>.

This is a PDF file of an article that has undergone enhancements after acceptance, such as the addition of a cover page and metadata, and formatting for readability, but it is not yet the definitive version of record. This version will undergo additional copyediting, typesetting and review before it is published in its final form, but we are providing this version to give early visibility of the article. Please note that, during the production process, errors may be discovered which could affect the content, and all legal disclaimers that apply to the journal pertain.

© 2021 THE AUTHORS. Published by Elsevier Inc on behalf of American Society for Biochemistry and Molecular Biology.



1. TITLE PAGE

TITLE: Lipid remodeling in response to methionine stress in MDA-MBA-468 triple-negative breast cancer cells

AUTHORS:

Stacey L. Borrego - 1

Johannes Fahrman – 2, 3

Jue Hou - 4

Da-Wei Lin -1

Bruce J. Tromberg – 4, 5

Oliver Fiehn - 2

Peter Kaiser - 1

1 – Department of Biological Chemistry, University of California, Irvine, Irvine, CA

2 – West Coast Metabolomics Center, University of California, Davis, Davis, CA

3 – Department of Clinical Cancer Prevention, University of Texas MD Anderson Cancer Center, Houston, TX

4 – Department of Biomedical Engineering, University of California, Irvine, Irvine, CA

5 – National Institute of Biomedical Imaging and Bioengineering, Bethesda, MD

CONTACT INFORMATION FOR CORRESPONDING AUTHOR: pkaiser@uci.edu

RUNNING TITLE: Lipid remodeling in response to methionine stress in cancer

ABBREVIATIONS:

- AAR - amino acid response
- ASNS - asparagine synthetase
- ATF4 - Activating Transcription Factor 4

- BHMT - Betaine--Homocysteine S-Methyltransferase
- CARS - coherent anti-Stokes Raman scattering
- CHOP - DDIT3, DNA damage inducible transcript 3
- DAG - diacylglycerol
- dLD - deuterium labeled lipid droplets
- ER - endoplasmic reticulum
- GCN2 - EIF2AK4, Eukaryotic Translation Initiation Factor 2 Alpha Kinase 4
- HCY - homocysteine
- LD – lipid droplet
- MB468 – shortened for MDA-MB-468 triple negative breast cancer cells
- MB468res-R8 – Resistant cell line derived from MB468, also referred to as “R8”
- MET - methionine
- MS - methionine synthase
- PC – phosphatidylcholine
- PE - phosphatidylethanolamine
- PEMT - phosphatidylethanolamine N-methyltransferase
- PERK - EIF2AK3, Eukaryotic Translation Initiation Factor 2 Alpha Kinase 3
- PLD - phospholipase D
- SAH - S - adenosylhomocysteine
- SAM - S - adenosylmethionine
- SRS - stimulated Raman scattering
- UPR - unfolded protein response

2. ABSTRACT AND KEYWORDS

ABSTRACT

Methionine is an essential amino acid and critical precursor to the cellular methyl donor S-adenosylmethionine. Unlike non-transformed cells, cancer cells have a unique metabolic requirement for methionine and are unable to proliferate in growth media where methionine is replaced with its metabolic precursor, homocysteine. This metabolic vulnerability is common among cancer cells regardless of tissue origin and is known as “methionine dependence”, “methionine stress sensitivity”, or the Hoffman effect. The response of lipids to methionine stress, however, is not well-understood. Using mass spectroscopy, label-free vibrational microscopy, and next-generation sequencing, we characterize the response of lipids to methionine stress in the triple-negative breast cancer cell line MDA-MB-468 and its methionine stress insensitive derivative, MDA-MB-468res-R8. Lipidome analysis identified an immediate, global decrease in lipid abundances with the exception of triglycerides and an increase in lipid droplets in response to methionine stress specifically in MDA-MB-468 cells. Furthermore, specific gene expression changes were observed as a secondary response to methionine stress in MDA-MB-468, resulting in a downregulation of fatty acid metabolic genes and an upregulation of genes in the unfolded protein response pathway. We conclude that the extensive changes in lipid abundance during methionine stress is a direct consequence of the modified metabolic profile previously described in methionine stress sensitive cells. The changes in lipid abundance likely results in changes in membrane composition inducing the unfolded protein response we observe.

KEYWORDS

Cancer metabolism; Homocysteine; Methionine; Methionine stress; Lipid metabolism; Lipid droplets; Phospholipids; Fatty acid metabolism; Triglycerides

3. INTRODUCTION

Methionine metabolism is an integral aspect in cellular function and is particularly important in cancer. Cancer cells that cannot proliferate in growth medium when methionine is replaced with its metabolic precursor, homocysteine, have been characterized as being “methionine dependent” or “methionine sensitive” (1). Previous studies indicate that cancer cells that become resistant to methionine stress or “methionine

independent", lose their transformed phenotype (2–4). Just as other metabolic alterations have been recognized as signatures of transformed cells, methionine metabolism is a unique metabolic requirement of cancer and is referred to as the Hoffman effect (1,5,6).

Methionine is an essential metabolite and is the precursor to S-adenosylmethionine (SAM), the principal methyl donor in the cell. SAM serves as a co-factor for a variety of methyltransferases that catalyze methylation events on DNA, RNA, proteins, and lipids (7). After donating its methyl group, SAM is converted into S-adenosylhomocysteine (SAH) and further processed to homocysteine (Hcy). At this point, Hcy can be catabolized in the transsulfuration pathway or methylated to regenerate methionine by way of methionine synthase (MS) and 5-methyltetrahydrofolate or betaine homocysteine methyltransferase (BHMT) and betaine, a product of choline. Both SAM and betaine are direct components of methionine metabolism and closely linked to phospholipid processing.

Phosphatidylcholine (PC) and phosphatidylethanolamine (PE) are the two most abundant lipid species in the cell and play an important structural role in cell membranes. Both PC and PE can be synthesized *de novo* through the two branches of the Kennedy pathway referred to as the CDP-choline and CDP-ethanolamine pathways, respectively (8,9). In normal cells, the majority of PC is synthesized through the CDP-choline pathway. Choline links methionine and PE metabolism as it is a precursor of betaine, which can regenerate methionine by way of BHMT, and it can be regenerated by PC catabolism via phospholipase D (PLD) (10). Interestingly, both choline and PC levels have been shown to be aberrantly upregulated in cancer along with many of their associated enzymes including PLD (11–14). In a less prominent pathway for PC synthesis, SAM is necessary for three sequential methylations on PE by the enzyme phosphatidylethanolamine N-methyltransferase (PEMT) (15,16). In both human and yeast studies, atypical Hcy or SAH levels lead to deregulation of phospholipid and triglyceride lipid metabolism (17,18). The level in which these two pathways can influence each other indicate a tight balance between methionine metabolism components and lipid synthesis.

The connection between methionine and lipid metabolic pathways have been extensively researched in the context of liver dysfunction and heart disease in the presence of high homocysteine levels. Recent work has extended these studies to different types of cancers of varying malignancy and thus the role of lipid metabolism and its connection to the methionine pathway is becoming more clear in tumor progression and metastasis (13,14,19). In a continued effort to understand the metabolic response during methionine stress, we performed lipidomic analyses in parallel to the untargeted metabolic and stable isotope-tracing study previously reported (4). Using the methionine-dependent, triple negative breast cancer cell line MDA-MB-468 (MB468) and its methionine-independent derived clone MDA-MB-468res-R8 (MB468res-R8 or R8), we have characterized the dynamic lipid response in cancer cells during methionine stress.

4. MATERIALS AND METHODS

Cell lines, growth conditions, and treatments

MB468 and MB468res-R8 cell lines were maintained in DMEM (Sigma-Aldrich, D0422) supplemented with 10% dialyzed FBS (Omega Scientific), 1.5 μ M cyanocobalmin (vitamin B12), 4 mM L- glutamine, 100 μ M L- cysteine (Fisher Scientific), and 100 μ M L-methionine (Sigma-Aldrich). In the case of methionine-free media, 370 μ M DL-homocysteine (Sigma-Aldrich) was added in the absence of methionine.

To induce ER stress, MB468 and MB468res-R8 cells were treated with the 1 μ M thapsigargin (Sigma-Aldrich, T9033) for 4 hours. To inhibit PERK activation, cells were treated with 1 μ M GSK2656157 (Millipore Sigma, 5.04651.0001) one hour prior to media switch or thapsigargin treatment and replaced in the new media.

Lipidome analysis

Lipidome analysis was performed by collecting 5×10^6 cells per sample -- pellet weights were measured for additional normalization. Each time point includes 4 biological replicates. Cell lysates were extracted as previously described (20). Briefly, 225 μ l of chilled methanol containing an internal standard mixture (PE

(17:0/17:0); PG (17:0/17:0); PC (17:0/0:0); C17 Spingosine; C17 Ceramide; SM (d18:0/17:0); Palmitic Acid-d3; PC (12:0/13:0); Cholesterol-d7; TG (17:0/17:1/17:0)-d5; DG (12:0/12:0/0:0); DG (18:1/2:0/0:0); MG (17:0/0:0/0:0); PE (17:1/0:0); LPC (17:0); LPE (17:1)) and 750 μ L of chilled MTBE (Methyl Tertiary Butyl Ether, Sigma-Aldrich) containing the internal standard 22:1 cholesteryl ester was added to cell lysates. Isotopically labeled internal standards included deuterated (d)- palmitate-d3, cholesterol-d7, and TG(17:0/17:0/17:0)-d5. Remaining lipid standards were selected as these were not identified in human plasmas during method development. We note that internal standards were used for normalization purposes and to correct for retention time drift, thereby increasing accuracy of annotations. Samples were shaken for 6 minutes at 4°C using an Orbital Mixing Chilling/Heating Plate (Torrey Pines Scientific Instruments) followed by the addition of 188 μ l of room temperature distilled water. Samples were vortexed, centrifuged, the upper layer transferred to a new 1.5 mL microcentrifuge tube and subsequently dried to completeness under reduced pressure. Upon complete dryness, samples were resuspended in methanol:toluene (90:10) with 50 ng/mL CUDA ((12-[[cyclohexylamino]carbonyl]amino]- dodecanoic acid, Cayman Chemical).

Lipid extracts were subsequently analyzed on an Agilent 1290A Infinity Ultra High Performance Liquid Chromatography system with an Agilent Accurate Mass-6530-QTOF in both positive and negative mode. The column (65°C) was a Waters Acquity UPLC CSH C18 (100 mm length x 2.1 mm internal diameter; 1.7 μ M particles) containing a Waters Acquity VanGuard CSH C18 1.7 μ M Pre-column. The solvent system included A) 60:40 v/v acetonitrile:water (LCMS grade) containing 10 mM ammonium formate and 0.1% formic acid and B) 90:10 v/v isopropanol:acetonitrile containing 10 mM ammonium formate and 0.1% formic acid. The gradient started from 0 min 15% (B), 0-2 min 30% (B), 2-2.5 min 48% (B), 2.5-11 min 82% (B), 11-11.5 min 99% (B), 11.5-12 min 99% (B), 12-12.1 min 15% (B), and 12.1-15 min 15% (B). The flow rate was 0.6 mL/min and with an injection volume of 1 μ L for ESI (+) and 5 μ L for ESI (-) mode acquisition. ESI capillary voltage was +3.5 kV and -3.5 kV with collision energies of 25 eV and 40 eV for MS/MS collection in positive and negative acquisition modes, respectively. Data was collected at a mass range of m/z 60-1700 Da with a spectral acquisition speed of 2 spectra per second. Method blanks and pooled bioreclamation plasma samples were included to serve as additional quality controls.

Data was processed using MZmine 2.10. All peak intensities are representative of peak heights. Peaks were annotated by matching experimental accurate mass MS/MS spectra to MS/MS libraries including Metlin-MSMS, NIST12, and LipidBlast (2). Spectral matching was automated using the MSPepSearch tool, and manually curated using the NIST Mass Spectral Search Program v.2.0g. Metabolite libraries were created, in positive and negative ionization modes, containing all confirmed identified compounds. MZmine's Custom database search tool was used to assign annotations based on accurate mass and retention time matching using a m/z tolerance of 10 ppm and a RT tolerance of 0.1 min.

CARS/SRS microscopy

MB468 and MB468res-R8 cells were seeded at 200,000 cells per plate, 24 hours prior to the start of the experiment in 35 mm glass bottom dishes (Fisher Scientific, NC9268399). Cells were rinsed twice with phosphate buffered saline (PBS) prior to a media switch to methionine media (Met+) or homocysteine media (Met-Hcy+) for 0, 0.5, 2, 4, or 12 hours. Cells were fixed prior to imaging by washing twice with PBS, treating with a 4% formaldehyde/PBS solution for 20 minutes at room temperature, washing with PBS three times, and storing cells at 4°C in PBS.

For lipid labeling experiments, MB468 and MB468res-R8 cells were seeded in 35 mm glass bottom dishes at 350,000 cells per plate, 12 hours prior to the start of the experimental time course. Cells were cultured in either *unlabeled glucose media* or *labeled glucose media* prepared with 100 μM L-methionine or 370 μM DL-homocysteine. *Unlabeled glucose media* contains 4.5 g/L of glucose and *labeled glucose media* contains 4.5 g/L of D-glucose-1,2,3,4,5,6,7- d_7 (Sigma-Aldrich, 552003). Recipe for *base media*: DMEM without glucose (Caisson Labs, DMP04-10LT) supplemented with 10% dialyzed FBS (Omega Scientific), 1.5 μM vitamin B12, 4 mM L- glutamine, 1 mM sodium pyruvate, 44 mM sodium bicarbonate, and *50x amino acid mix*. Recipe for *50x amino acid mix*: L-arginine HCl 0.084 g/L, cysteine HCl 0.018 g/L, glycine 0.03 g/L, L-histidine HCl 0.042 g/L, L-isoleucine 0.105 g/L, L-leucine 0.105 g/L, L-phenylalanine 0.066 g/L, L-serine 0.066 g/L, L-threonine 0.095 g/L, L-tryptophan 0.016 g/L, and L-valine g/L.

Lipid synthesis analysis was performed by culturing cells in *unlabeled glucose media* with methionine for 12 hours, washing cells twice with PBS, adding *labeled glucose media* with homocysteine for 0, 0.5, 2, 4, or 12 hours, and then fixing with formaldehyde as described above. Lipid degradation analysis was performed by culturing cells in *labeled glucose media* with methionine for 12 hours, washing cells twice with PBS, adding *unlabeled glucose media* with homocysteine, and then fixing with formaldehyde as described above.

Cells were imaged using a 76-MHz mode-locked Nd:vanadate laser that provides a beam at 1,064 nm functioning as the Stokes beam and a second harmonic generated beam at 532 nm to pump an optical parametric oscillator. The pump beam generated by the optical parametric oscillator is spatially and temporally overlapped with the Stokes beam and sent to the microscope. The two beams are focused on the cells through a 60 \times , 1.2 numerical aperture water objective lens. The generated CARS signals are collected through the condenser and focused onto a Hamamatsu photomultiplier tube with a 650 \pm 50 nm bandpass filter in front. The SRS signals are collected and detected with a Thorlab photodiode (FDS1010, Thorlabs, Inc.) and a high O.D. bandpass filter (Semrock, Inc.) Both signals were measured in order to identify the cells and their morphology using the non-resonant background (CARS) and quantify lipid content (SRS, which is background free).

Gene expression analysis

Total RNA from MB468 and MB468res-R8 cells was extracted using the RNeasy Plus Mini Kit (Qiagen, 74134) and library preparation was performed using the TruSeq RNA Library Preparation Kit v2 (Illumina, RS-122-2001 and RS-122-2002) with the ERCC RNA Spike-In mix (ThermoFisher, 4456740) to control for sample preparation variation. PolyA selected libraries were sequenced using single-end, 100 bp reads at the University of California, Irvine Genomics High Throughput Facility on an Illumina HiSeq 4000 system.

Raw reads were aligned to a custom reference sequence, defined as the union of the human reference genome (GRCh38/hg38, UCSC Genome Browser) and the ERCC spike-in sequences (<http://tools.invitrogen.com/downloads/ERCC92.fa>) using HISAT2 alignment software (21). Number of reads

mapped to each gene feature was quantified by featureCounts in the Rsubread package and unwanted sample variation was determined by RUVSeq (22,23). Read counts were normalized and differential gene expression analysis was performed using DESeq2 (24). Pathway enrichment analysis was conducted via gene-set enrichment analysis (GSEA) (25). GSEA was performed on the DESeq2 normalized expression signals via a running-sum statistic procedure to determine the enrichment of biological pathways from the Molecular Signature Database Hallmark Gene Set Collection (26).

Real-time quantitative PCR analysis

Total RNA from MB468 and MB468res-R8 cells was extracted using the RNeasy Plus Mini Kit (Qiagen, 74134). Equal amounts (1.5 µg) of RNA was reverse transcribed using SuperScript II Reverse Transcriptase (Invitrogen) per manufacturer's instructions – with the exception of using 0.3 uL of SuperScript II per reaction. Gene expression was quantified using SYBR Green (Bio-Rad, 1725124) and Bio-Rad CFX Connect real-time PCR detection system. Primer sequences are as follows: CHOP (forward) 5'-AGAACCAGGAAACGGAAACAGA -3', (reverse) 5'-TCTCCTTCATGCGCTGCTTT-3'; ASNS (forward) 5'-TGCACCATGTGTGGCATTG-3'; (reverse) 5'-AGCAGCAGTTGGTGTATCCAT-3'. Relative gene expression to Met+ control sample was determined using CFX Maestro software (Bio-Rad).

5. RESULTS

Methionine stress induces a global lipid response

Unlike normal, non-transformed cells, the majority of cancer cells are unable to survive in growth media where methionine has been replaced with its metabolic precursor, homocysteine (4,27–30). To elucidate the role of methionine in cancer, we use a methionine dependent and independent cell pair: MB468 and MB468res-R8, respectively. While reversion of a transformed, methionine-dependent cell to a non-transformed, methionine-independent phenotype is a rare event, MB468 cells are one of the few cell lines capable of such a reversion. As previously reported by Hoffman and colleagues (3), we were able to generate methionine-independent

clones by culturing the parental cell line, MB468, in homocysteine media (Met-Hcy+) for a prolonged period of time (4,30,31). The revertant clone, MB468res-R8 was selected as a control for these studies as it most closely resembles the parental cell in both morphology and proliferation rate while exhibiting a non-transformed, methionine-independent phenotype (4,30).

Using MB468 and MB468res-R8 cells, we previously reported immediate metabolic changes in response to homocysteine media in a cell line specific manner (4). We further expanded on these metabolic findings and focused on the lipidomic response during methionine stress. Both MB468 and MB468res-R8 cells were cultured in normal, methionine media (Met+), or transitioned to homocysteine media (Met-Hcy+) for 2, 4, 8, 12, and 24 hours, and lipids were measured by UHPLC-QTOF (FIGURE 1). We focus on early time points to avoid cell cycle effects imposed by the arrested growth of MB468 and continued proliferation of MB468res-R8 in Met-Hcy+ media (4,30). Within two hours of exposure to Met-Hcy+ media, we observe a remarkable decrease in all lipid classes in MB468 cells (FIGURE 1A). Interestingly, triglyceride abundance levels begin a steady trend of recovery as early as 4 hours post-media switch, unlike the majority of lipid classes measured. In contrast to MB468 cells, the methionine independent MB468res-R8 cells show a global increase in lipid abundance with the exception of triglycerides (FIGURE 1B). The decline in MB468res-R8 triglyceride levels is not as immediate as observed in MB468 cells, it takes up to 4 hours in Met-Hcy+ media to observe a decline in the majority of triglyceride species. The contrast in global lipid behavior between the two cell lines may suggest differential coping mechanisms in response to methionine stress, or the remodeling of lipid behavior in MB468 as opposed to the expected general lipid increase/decrease trend for a proliferating cell in MB468res-R8. Importantly, these effects are initiated long before cell cycle arrest is induced and are thus autonomous responses in lipid metabolism characteristic for the methionine dependent state (30).

Phosphatidylcholine and phosphatidylethanolamine abundance acutely decrease in response to methionine stress

Phospholipids are the largest class of lipids in the cell and their synthesis is directly connected to methionine metabolism (FIGURE 2A). Both phosphatidylcholine (PC) and phosphatidylethanolamine (PE) are synthesized

de novo in the endoplasmic reticulum via the Kennedy pathway using choline and ethanolamine, respectively (8). Choline not only serves as a precursor to PC, but provides cellular betaine that can remethylate homocysteine for methionine regeneration (7,32). As indicated by global lipid analysis (FIGURE 1), MB468 and MB468res-R8 levels of PC (FIGURE 2B) and PE (FIGURE 2C) respond to Met-Hcy⁺ media in distinct fashions. In MB468 cells, PC and PE abundance levels drop below 90% and 80%, respectively, within 2 hours post-media switch. However, lipid abundances in MB468res-R8 cells indicate a steady increase over time and return to starting abundance levels by 24 hours – following an expected lipid abundance trajectory for proliferating cells.

PE can be methylated three times by PEMT using SAM as a methyl donor to synthesize PC (FIGURE 2A) (9). Although newly synthesized SAM levels are reduced during methionine stress, the PC/PE ratio increases within 2 hours post-media switch in MB468 cells (FIGURE 2D) (4). This result excludes SAM limitation as a driving factor for PC and PE reduction, because if SAM were the limiting factor in PC synthesis, a decrease in the PC to PE ratio would be observed (33). However, the PC/PE ratio increase is likely due to a greater loss of PE levels than PC as previously noted. While declining abundance is observed in both PC and PE in response to Met-Hcy⁺ media, the considerable reduction of PE may indicate a greater sensitivity in this lipid class to methionine stress as has been shown for ferroptosis (34).

It is interesting to note phospholipid abundances in time-zero samples cultured in Met⁺ media (TABLE 1). In breast cancer, PC and PE are detected at elevated levels as compared to normal cell and tissue samples and fittingly PE levels are approximately 3-times higher in MB468 than MB468res-R8 cells (35). In contrast, PC levels are comparable between the two cell lines. The increase in PE in MB468 may put these cells in a vulnerable state as the PC/PE ratio is modified and perhaps less resilient to stress, making the cells more susceptible to damage by oxidative stress and inducing an ER stress response by lipid disequilibrium (36).

Both diacylglycerol (DAG) and choline contribute to the biosynthesis of PC and PE in the Kennedy pathway in the ER (9). With its own unique metabolic response to Met-Hcy⁺ media, DAGs gradually decrease over time in MB468 cells whereas little change is observed in MB468res-R8 cells (FIGURE 2E). Interestingly, choline

abundances increase after 12 hours post-media switch in MB468 and within 4 hours in MB468res-R8 – a similar response to Met-Hcy⁺ media as previously reported on reduced and oxidized glutathione (FIGURE 2F) (4). The unique profile of DAGs in MB468 may reflect its depletion as the cell attempts to restore declining PC abundances and choline levels increase to meet the sudden demand of PC synthesis. Furthermore, DAG depletion could also be a result of its use as a precursor for other lipid species including phosphatidic acid and triglycerides (37).

Oxidative stress induced lipid peroxidation may influence lipid remodeling

The immediate decrease in global lipid abundances in response to Met-Hcy⁺ media likely indicates lipid damage. Lipid peroxidation is a process that targets unsaturated lipids in the presence of free radicals or prooxidants and is one potential route for lipid damage when cells are cultured in Met-Hcy⁺ media. In the presence of oxidative stress, prooxidants attack unsaturated lipids resulting in lipid radicals. Lipid peroxy radicals are produced when oxygen reacts with the lipid radical and these reactive lipid species propagate damage by reacting with more unsaturated lipids. Neither lipid radicals nor lipid peroxy radicals are identified as the original lipid species since the mass (m/z) is altered and therefore a different spectrum for the newly formed oxidized lipid species is generated (38,39). In our study, we did not employ mass spectrometry techniques to measure oxidized lipids, however we have previously measured oxidized lipids in individual cells using fluorescence lifetime imaging (FLIM) and shown a rapid and dramatic increase in oxidized lipids when MB468 cells are shifted to homocysteine medium (4). We therefore suggest that the immediate decrease in lipid abundance is due to an increase in oxidized lipid species that are no longer interpreted as the original lipid species. The lipid peroxidation reaction can be terminated in the presence of an antioxidant such as reduced glutathione, a cellular oxidant readily available to neutralize casualties of oxidation (40,41).

As previously reported, both reduced and oxidized glutathione levels increase in response to homocysteine media induced oxidative stress in MB468 and MB468res-R8 cells (4). Interestingly, glutathione levels increase in MB468 cells by 12 hours post-media switch while MB468res-R8 cells respond earlier within 4 hours. This delayed glutathione response in MB468 may allow lipid peroxidation to occur, decreasing phospholipid

abundances immediately. Upon glutathione up-regulation in MB468, phospholipids attempt to recover to starting levels without success by 24 hours post-media switch (FIGURE 2B and 2C). Up-regulation of glutathione suggest a response to oxidative stress, which is further validated by oxidative stress assays in MB468 and MB468res-R8 cells that indicate a mild reduction in ROS levels over time in homocysteine media (Supplemental FIGURE S1).

It is worth noting that MB468res-R8 cells may be able to further circumvent lipid damage and facilitate recovery with an increase in glutamine. As glutamine can contribute to the cysteine pool for GSH synthesis and thus cellular redox homeostasis, we observe an early increase in glutamine within 2 hours post-media switch ($p = .007$), which coordinates with our previous cysteine results (4). In MB468 cells, however, no significant changes are observed (ANOVA $p = .747$). It is likely that the increased abundance of glutamine also contributes to the spike at 2 hours post-media switch observed in alpha-ketoglutarate ($p \leq .001$), citric acid ($p = .01084$), and malic acid ($p \leq .001$) in MB468res-R8 cells. These concomitant increases in TCA metabolites and precursors for lipid metabolism may help alleviate the consequences of methionine stress in MB468res-R8 cells.

Triglycerides have a distinct response to methionine stress

An immediate global lipid response to methionine stress is only observed in MB468 cells, yet both cell lines indicate a unique behavior in triglycerides as compared to other lipid species. Here we focus on triglycerides from the lipidomic experiment summarized in FIGURE 1. To understand the overall response of triglycerides over time in Met-Hcy+ media, all MB468 and MB468res-R8 triglyceride lipid abundances were clustered and four distinct trends were identified (FIGURE 3A) (42). Each cluster represents a unique trend and there is remarkably minimal to no overlap of cell origin, confirming the distinct triglyceride response in methionine dependent and independent cells. MB468 triglycerides typically decline in abundance within 2 hours post-media switch and attempt to recover by 8 (cluster 1) or 24 hours (cluster 2) (FIGURE 3A). MB468res-R8 cells also separate into two unique clusters, one with declining abundances by 4 hours post-media switch (cluster 3) and another that first increases in abundance at 2 hours post-media switch then decreases at 12 hours (cluster 4)

4) (FIGURE 3A). These differences in triglyceride trajectories indicate that both cell lines have a unique response to Met-Hcy+ media and a unique feature of triglycerides segregates the cell-dependent response.

Triglycerides consist of a glycerol backbone and three fatty acid tails of varying chain length and unsaturated, double bonds. In order to determine any unique features of triglycerides that may be most affected during methionine stress, correlation tests were performed on triglycerides in MB468 and MB468res-R8. We first tested lipid species with a combined tail length between 50 and 58 carbons and a single unsaturated bond. Our results indicate that both MB468 and MB468res-R8 triglycerides with a combined tail length of 50 carbons have unique profiles that only correlate with lipid species within each cell line (Pearson correlation coefficient $r = .56$) (FIGURE 3B - top left panel). As the combined tail length increases to a combined length of 58 carbons, the profiles of both cell lines begin to look more similar (Pearson correlation coefficient $r = .87$) (FIGURE 3B - bottom left panel). Next, we performed correlation tests on triglycerides in MB468 and MB468res-R8 with a combined tail length between 50 and 58 carbons and 4 unsaturated bonds. Our results indicate distinct profiles in MB468 and MB468res-R8 cells for lipid species with a combined tail length of 50 (Pearson correlation coefficient $r = .03$) (FIGURE 3B - top right panel). Interestingly, at a combined tail length of 58 carbons, the lipid profiles in MB468 and MB468res-R8 become inversely correlated (Pearson correlation coefficient $r = -.68$) (FIGURE 3B - bottom right panel). These data suggest a particularly unique response of longer chain, heavily desaturated triglycerides in methionine dependent and independent cells.

Further analysis of cluster composition indicates that the number of unsaturated bonds is the unique feature separating the triglyceride response to Met-Hcy+ media (FIGURE 3A). Triglycerides in MB468 are primarily represented in clusters 1 and 2 (FIGURE 3A); between these two clusters, cluster 1 mostly contains single unsaturated lipids whereas cluster 2 contains lipid species with 3 or more unsaturated bonds (FIGURE 3C). MB468res-R8 predominantly composes clusters 3 and 4 (FIGURE 3A), with a distinct division of lipids in cluster 3 containing only lipid species with 1 to 3 unsaturated bonds and a range of unsaturated lipid species in cluster 4 (FIGURE 3D).

This data indicates that MB468 and MB468res-R8 cells have unique lipid profiles in response to Met-Hcy+ over time regarding abundance levels. Both cell lines have unique profiles for lipid species with a single unsaturated double bond compared to four unsaturated, double bonds with little to no difference in profiles with the same number of unsaturated bonds but of varying combined tail lengths.

Lipid droplets accumulate in MB468 in response to methionine stress

In addition to modified triglyceride behavior, an increase in lipid droplet abundance is also observed in MB468 cells in response to methionine stress. Lipid droplets are dynamic organelles originating from the ER and comprised of a neutral lipid core of triglycerides and cholesterol esters surrounded by a phospholipid monolayer (43). Using coherent anti-Stokes Raman scattering (CARS) and stimulated Raman scattering (SRS) microscopy to specifically detect C-H bonds in fatty acids, we quantify lipid content per cell (44). Using this method, lipid abundances are measured as the number of pixels that belong to lipid droplets in a cell over the total pixel numbers of the entire cell (45).

Both MB468 and MB468res-R8 cells were cultured in Met+ (0 hour) or Met-Hcy+ media (0.5, 2, 4, 24 hours) and fixed samples were analyzed by CARS microscopy (FIGURE 4A and 4B). In normal culturing conditions (Met+), MB468res-R8 cells have twice the lipid content per cell of MB468 cells ($p \leq .001$). However, lipid content per cell does not change in MB468res-R8 cells upon Met-Hcy+ media switch (ANOVA $p = .93$). In contrast, MB468 lipid content per cell increases within 30 minutes post-media switch to Met-Hcy+ and elevated abundance levels remain stable after 2 hours exposure to methionine stress (ANOVA $p \leq .001$). It is important to note that both lipid droplets and triglycerides have been linked directly with oxidative phosphorylation, for which we observe a down-regulation in both MB468 and MB468res-R8 cells (4,46,47). Thus, the differences observed in both triglyceride trends and lipid droplet accumulation in response to homocysteine media are likely not a result of impaired oxidative phosphorylation alone.

To better understand the remodeling of lipid metabolism in MB468 – specifically the acute decrease in lipid abundance (FIGURE 1A) and increase in lipid droplets (FIGURE 4A and 4B), we combined SRS and CARS

microscopy methods with deuterium labeled glucose as a lipid precursor in order to label and monitor lipid dynamics (48,49). Two experiments were designed to understand the mechanism of lipid degradation and synthesis during methionine stress. First, we measured lipid degradation in MB468 and MB468res-R8 by labeling lipids with deuterated glucose in Met⁺ media for 12 hours then switching the cell cultures to unlabeled Met⁺ (0 hour) or Met-Hcy⁺ media (0.5, 2, 4, 12 hours) (FIGURE 4C - *left panel* and 4D). Fixed samples were measured using SRS and CARS microscopy for deuterium labeled lipid droplets (dLD) and total lipid pool (LD). Both cell lines were labeled to approximately ~ 20% after the 12 hour labeling period and lipid content (dLD/LD) was normalized to the unlabeled, time-zero sample. Both cell lines presented similar decreasing trajectories over time, although MB468res-R8 cells lose their label faster within the first 30 minutes post-media switch (MB468 – 0.16, MB468res-R8 – 0.13). However, labeled lipid content per cell ratios between the cells maintain a 0.03 difference over time. Thus, lipid degradation appears very similar in both methionine dependent and independent cell lines.

Alternatively, lipid synthesis was determined by monitoring the increased presence of deuterium labeled lipid content per cell over time. Both MB468 and MB468res-R8 cell lines were cultured in Met⁺ (0 hour) or Met-Hcy⁺ media prepared with deuterium labeled glucose (0.5, 2, 4, 12 hours) and imaged by SRS and CARS microscopy (FIGURE 4C - *right panel* and 4E). MB468 cells respond to the Met-Hcy⁺ media shift with a rapid increase in lipid synthesis up to 4 hours post-media switch as compared to MB468res-R8. However, lipid synthesis plateaus after 2 hours in Met-Hcy⁺ media whereas MB468res-R8 continue to synthesize lipids resulting in significantly more lipid synthesis after 12 hours post-media switch. With similar rates of lipid degradation between MB468 and MB468res-R8 cells, it appears that lipid synthesis is the predominate responding pathway to methionine stress. The immediate acceleration of synthesis is likely a response to compensate for acute global loss of lipids (FIGURE 1A), but the increased rate of synthesis is not sustained in methionine dependent cells; thus, leading to overall lower lipid production as compared to methionine independent MB468res-R8 cells (FIGURE 4B).

Gene expression during methionine stress

To further elucidate the metabolic response to methionine stress, gene expression analysis was performed on MB468 and MB468res-R8 cells cultured in Met⁺ (0 hour) or Met-Hcy⁺ media (2 or 12 hours). Although MB468 and MB468res-R8 cells originate from the same genetic background, their expression profile in methionine medium was surprisingly different. When these cells were shifted to Met-Hcy⁺ medium, expression programs in both cell lines were significantly remodeled to adapt to the modified growth conditions. Expression changes in response to methionine stress were specific for MB468 and MB468res-R8 cells. Expression changes were only observed after prolonged culturing under methionine stress, indicating that the observed rapid effects on lipid profiles were likely independent from transcription (FIGURE 5A and TABLE 2). We applied gene set enrichment analysis using hallmark gene set collections and observed a prominent down-regulation of fatty acid (FA) metabolic genes in MB468 cells at 12 hours post-media switch as compared to MB468res-R8 cells (FIGURE 5B) (25,26,50). Further analysis of gene ontology FA pathways indicated a two-fold down-regulation of 22.3% of genes in FA biosynthetic processes and 15.9% of genes in the FA beta-oxidation pathway at 12 hours post-media switch as compared to time-zero (FIGURE 5C and TABLE 2). MB468 up-regulated genes in FA biosynthetic and beta-oxidation processes are minimal – 5.6% and 2.3%, respectively. As previously noted, effects on transcription are mostly delayed as exemplified by the gene expression profiles of FASN, ELOVL6, and ACLY in the FA biosynthetic processes pathway and CRAT, ACADM, and ACADS in the FA beta-oxidation pathway (TABLE 2). Therefore, it seems that a global shut down in lipid metabolism is a consequence of methionine stress with a more pronounced effect in gene synthesis at 12 hours post-media switch.

The global lipid response, remodeled triglyceride behavior, decrease in lipid synthesis, and increase in lipid droplet abundance suggest that methionine stress may largely affect functions of the endoplasmic reticulum (ER). To further investigate this connection, we looked into the unfolded protein response (UPR), which is a cellular stress response pathway related to the ER and the ER stress response. Gene set enrichment analysis indicates no uniform response in UPR as subsets of genes are both up-regulated and down-regulated by 12 hours post-media switch (FIGURE 5D). However, key genes found down-stream of the UPR, including C/EBP homologous protein (CHOP), asparagine synthetase (ASNS), GADD34, and FGF21 were up-regulated (FIGURE 5E – 5H).

To understand the response of CHOP and ASNS, quantitative PCR was performed on MB468 and MB468res-R8 cells cultured in Met+, Met-Hcy+, or Met+Hcy+ medias. Cells were also treated with the ER stress inducing agent thapsigargin as a positive control (FIGURE 5G and 5H). CHOP is a multifunctional transcription factor that responds to a wide variety of cellular stresses and is well-known to be up-regulated during UPR and ER stress responses (51). As expected, CHOP was up-regulated in response to thapsigargin in both MB468 and MB468res-R8 (FIGURE 5G). Interestingly, CHOP was also up-regulated in MB468, but not MB468res-R8, cells when cultured in Met-Hcy+ media. Furthermore, asparagine synthetase (ASNS) is transcriptionally regulated by activating transcript 4 (ATF4) and CHOP during the UPR and amino acid response (AAR) (52,53). While ASNS expression levels are moderately elevated in response to thapsigargin in both MB468 and MB468res-R8, a 2-fold up-regulation is observed in MB468 cultured in Met-Hcy+ media (FIGURE 5H). Both CHOP and ASNS up-regulation is observed during methionine stress in MB468 cells, suggesting full or partial activation of multiple stress response pathways, including ER stress, UPR, and the AAR.

6. DISCUSSION

We monitored lipid species during the initial phases of methionine stress response in triple negative breast cancer cells MDA-MB-468. This cell line has been selected as a model because genetically largely identical, but methionine independent derivatives MB468res-R8 have been developed (4,30,31). We found extensive and fast lipid remodeling in response to methionine stress in the breast cancer cell line MB468. We show an immediate, global decrease in lipid abundances with the exception of single unsaturated triglycerides, that was specific for methionine dependent cancer cells. Furthermore, lipid content per cell increase in response to methionine stress specifically in MB468 but not MB468res-R8 cells. Gene expression changes are observed as a later response, indicating an overall decrease in fatty acid metabolic genes and an up-regulation of specific genes downstream of the unfolded protein response pathway, which was not observed in methionine independent cells.

Interestingly, numerous reports indicate that homocysteine influences triglyceride biosynthesis and export, ER stress and UPR induction, and gene expression in cardiac and hepatic systems (54–56). Here we see a comparable response profile in a cancer specific setting that investigates the cell proliferation arrest and apoptosis when cancer cells are shifted to Met-Hcy+ medium. Notably, these effects of homocysteine medium on cancer cells is not related to the presence of homocysteine but a manifestation of changed remodeled metabolism when methionine is replaced by homocysteine (6). This is also evident from UPR induction studies where addition of homocysteine to methionine containing medium has no effect on CHOP or ASNS induction, whereas Met-Hcy+ medium leads to CHOP and ASNS induction (FIGURE 5G and 5H).

We have previously reported that methionine stress in breast cancer cells can be rescued with S - adenosylmethionine supplementation, suggesting that the impact on the one-carbon cycle and cellular methylation is causing a major cellular stress (30). We therefore expected to see an impact of phosphatidylcholine levels because methylation of phosphatidylethanolamine is hampered. However, we did not observe any change in the PC/PE ratio, but rather fast reduction of both phospholipid species specifically in MB468 cells. Our previous metabolite tracing studies suggested that cancer cells redirect homocysteine to the transsulfuration pathway to increase the synthesis of glutathione and compensate for increased oxidative stress under these growth conditions (1,4). We also observed an increase in lipid oxidation based on FLIM studies (4). We therefore hypothesize that the very rapid loss of several lipid species in MB468 cells may be due to a burst in lipid oxidation, which removes these species from detection by our mass spectrometric approach. We believe this is a likely scenario because lipid synthesis is rapidly increasing during this early phase of methionine stress, and is in fact more active in MB468 than in MB468res-R8 cells.

The robust effect on lipid content and the rapid change early after cancer cells were shifted to homocysteine medium was surprising. Most of these effects are much earlier than gene expression effects are observed. It is therefore likely that the in lipid composition in cancer cells during methionine stress is a direct effect of the remodeled metabolism we observed in previous studies (4). Additional changes we observed in transcription profiles, lipid droplet accumulation, and UPR induction are likely adaptations or consequences of the initial impact by metabolic remodeling to adjust to methionine stress. Future studies will be important to dissect

signals that induce these adaptive changes to fully understand the role of lipid metabolism in the cancer specific metabolic dependence on methionine.

7. DATA AVAILABILITY STATEMENT

All data are contained within the article – lipidomic results are attached as supplemental data. RNA-sequencing data and results have been deposited in the NCBI Gene Expression Omnibus (GEO) with accession number GSE155955.

8. ACKNOWLEDGEMENTS/GRANT SUPPORT

This research was funded by pilot project funding by the West Coast Metabolomics Center as part of NIH-DK097154 and by National Institute of Health grants R01GM128432 and R21CA242270. The content is solely the responsibility of the authors and does not necessarily represent the official views of the National Institutes of Health.

9. REFERENCES

1. Kaiser P. Methionine Dependence of Cancer. *Biomol* 2020, Vol 10, Page 568. 2020 Apr;10(4):568.
2. Hoffman RM, Jacobsen SJ, Erbe RW. Reversion to methionine independence by malignant rat and SV40-transformed human fibroblasts. *Biochem Biophys Res Commun.* 1978;82(1):228–34.
3. Hoffman RM, Jacobsen SJ, Erbe RW. Reversion to methionine independence in simian virus 40-transformed human and malignant rat fibroblasts is associated with altered ploidy and altered properties of transformation. *Proc Natl Acad Sci U S A.* 1979;76(3):1313–7.
4. Borrego SL, Fahrman J, Datta R, Stringari C, Grapov D, Zeller M, et al. Metabolic changes associated with methionine stress sensitivity in MDA-MB-468 breast cancer cells. *Cancer Metab [Internet].* 2016;4(1):1–17. Available from: <http://dx.doi.org/10.1186/s40170-016-0148-6>
5. Hanahan D, Weinberg RA. Hallmarks of cancer: The next generation. *Cell [Internet].* 2011;144(5):646–74. Available from: <http://dx.doi.org/10.1016/j.cell.2011.02.013>
6. Hoffman RM. Methionine dependence of cancer and aging : methods and protocols. 329 p.
7. Finkelstein JD, Martin JJ. Methionine Metabolism in Mammals. 1984;259(15):9508–13.
8. DeLong CJ, Shen YJ, Thomas MJ, Cui Z. Molecular distinction of phosphatidylcholine synthesis between the CDP- choline pathway and phosphatidylethanolamine methylation pathway. *J Biol Chem.* 1999;274(42):29683–8.
9. Gibellini F, Smith TK. The Kennedy pathway-de novo synthesis of phosphatidylethanolamine and phosphatidylcholine. *IUBMB Life.* 2010;62(6):414–28.

10. Banno Y. Regulation and possible role of mammalian phospholipase D in cellular functions. *J Biochem.* 2002;131(3):301-6.
11. Glunde K, Jie C, Bhujwala ZM. Molecular causes of the aberrant choline phospholipid metabolism in breast cancer. *Cancer Res.* 2004;64(12):4270-6.
12. Xu X, Gammon MD, Zeisel SH, Yin LL, Wetmur JG, Teitelbaum SL, et al. Choline metabolism and risk of breast cancer in a population-based study. *FASEB J.* 2008;22(6):2045-52.
13. Glunde K, Bhujwala ZM, Ronen SM. Choline metabolism in malignant transformation. *Nat Rev Cancer.* 2011;11(12):835-48.
14. Cao MD, Dopkens M, Glunde K. Glycerophosphodiester phosphodiesterase domain containing 5 (GDPD5) expression correlates with malignant choline phospholipid metabolite profiles in human breast cancer. 2012;25(9):1022-42.
15. Daum G, Lees ND, Bard M, Dickson R. Biochemistry, cell biology and molecular biology of lipids of *Saccharomyces cerevisiae*. *Yeast.* 1998;14(16):1471-510.
16. Watkins SM, Zhu X, Zeisel SH. Phosphatidylethanolamine-N-methyltransferase Activity and Dietary Choline Regulate Liver-Plasma Lipid Flux and Essential Fatty Acid Metabolism in Mice. *J Nutr.* 2003;133(11):3386-91.
17. Malanovic N, Streith I, Wolinski H, Rechberger G, Kohlwein SD, Tehlivets O. S-adenosyl-L-homocysteine hydrolase, key enzyme of methylation metabolism, regulates phosphatidylcholine synthesis and triacylglycerol homeostasis in yeast: Implications for homocysteine as a risk factor of atherosclerosis. *J Biol Chem.* 2008;283(35):23989-99.
18. Tehlivets O, Malanovic N, Visram M, Pavkov-Keller T, Keller W. S-adenosyl-L-homocysteine hydrolase and methylation disorders: Yeast as a model system. *Biochim Biophys Acta - Mol Basis Dis [Internet].* 2013;1832(1):204-15. Available from: <http://dx.doi.org/10.1016/j.bbadis.2012.09.007>
19. Breillout F, Antoine E, Poupon MF. Methionine Dependency of Malignant Tumors: A Possible Approach for Therapy. *J Natl Cancer Inst.* 1990;82(20):1628-32.
20. Fahrman J, Grapov D, Yang J, Hammock B, Fiehn O, Bell GI, et al. Systemic alterations in the metabolome of diabetic NOD mice delineate increased oxidative stress accompanied by reduced inflammation and hypertriglyceremia. *Am J Physiol - Endocrinol Metab.* 2015;308(11):E978-89.
21. Kim D, Paggi JM, Park C, Bennett C, Salzberg SL. Graph-based genome alignment and genotyping with HISAT2 and HISAT-genotype. *Nat Biotechnol [Internet].* 2019;37(8):907-15. Available from: <http://dx.doi.org/10.1038/s41587-019-0201-4>
22. Liao Y, Smyth GK, Shi W. The R package Rsubread is easier, faster, cheaper and better for alignment and quantification of RNA sequencing reads. *Nucleic Acids Res.* 2019;
23. Risso D, Ngai J, Speed TP, Dudoit S. Normalization of RNA-seq data using factor analysis of control genes or samples. *Nat Biotechnol.* 2014;32(9):896-902.
24. Love MI, Huber W, Anders S. Moderated estimation of fold change and dispersion for RNA-seq data with DESeq2. *Genome Biol.* 2014;15(12):1-21.
25. Subramanian A, Tamayo P, Mootha VK, Mukherjee S, Ebert BL, Gillette MA, et al. Gene set enrichment analysis: A knowledge-based approach for interpreting genome-wide expression profiles. *Proc Natl Acad Sci U S A.* 2005;102(43):15545-50.
26. Liberzon A, Birger C, Thorvaldsdóttir H, Ghandi M, Mesirov JP, Tamayo P. The Molecular Signatures Database Hallmark Gene Set Collection. *Cell Syst.* 2015;1(6):417-25.
27. Stern PH, Wallace CD, Hoffman RM. Altered methionine metabolism occurs in all members of a set of diverse human tumor cell lines. *J Cell Physiol.* 1984;119(1):29-34.
28. Mechem JO, Rowitch D, Wallace CD, Stern PH, Hoffman RM. The metabolic defect of methionine dependence occurs frequently in human tumor cell lines. *Biochem Biophys Res Commun.* 1983;117(2):429-34.
29. Lien EC, Ghisolfi L, Geck RC, Asara JM, Toker A. Oncogenic PI3K promotes methionine dependency in breast cancer cells through the cystine-glutamate antiporter xCT. *Sci Signal.*

- 2017 Dec;10(510).
30. Booher K, Lin DW, Borrego SL, Kaiser P. Downregulation of Cdc6 and pre-replication complexes in response to methionine stress in breast cancer cells. *Cell Cycle*. 2012;11(23):4414–23.
 31. Borrego SL, Lin D-W, Kaiser P. Isolation and Characterization of Methionine-Independent Clones from Methionine-Dependent Cancer Cells. *Methods Mol Biol*. 2019;1866:37–48.
 32. Chadwick LH, McCandless SE, Silverman GL, Schwartz S, Westaway D, Nadeau JH. Betaine-homocysteine methyltransferase-2: cDNA cloning, gene sequence, physical mapping, and expression of the human and mouse genes. *Genomics*. 2000;70(1):66–73.
 33. Walker AK, Jacobs RL, Watts JL, Rottiers V, Jiang K, Finnegan DM, et al. A conserved SREBP-1/phosphatidylcholine feedback circuit regulates lipogenesis in metazoans. *Cell*. 2011;147(4):840–52.
 34. Kagan VE, Mao G, Qu F, Angeli JPF, Doll S, Croix CS, et al. Oxidized arachidonic and adrenic PEs navigate cells to ferroptosis. *Nat Chem Biol*. 2017;13(1):81–90.
 35. Sakai K, Okuyama H, Yura J, Takeyama H, Shinagawa N, Tsuruga N, et al. Composition and turnover of phospholipids and neutral lipids in human breast cancer and reference tissues. *Carcinogenesis*. 1992;13(4):579–84.
 36. Patel D, Witt SN. Ethanolamine and Phosphatidylethanolamine: Partners in Health and Disease. *Oxid Med Cell Longev*. 2017;2017.
 37. Carrasco S, Mérida I. Diacylglycerol, when simplicity becomes complex. *Trends Biochem Sci*. 2007;32(1):27–36.
 38. Spickett CM, Pitt AR. Oxidative lipidomics coming of age: Advances in analysis of oxidized phospholipids in physiology and pathology. *Antioxidants Redox Signal*. 2015;22(18):1646–66.
 39. Koelmel JP, Ulmer CZ, Jones CM, Yost RA, Bowden JA. Common cases of improper lipid annotation using high-resolution tandem mass spectrometry data and corresponding limitations in biological interpretation. *Biochim Biophys Acta - Mol Cell Biol Lipids*. 2017;1862(8):766–70.
 40. Halliwell B, Chirico S. Lipid peroxidation : and significanc & 3 its mechanism ,. *Am J Clin Nutr*. 1993;57:715S-725S.
 41. Ayala A, Muñoz MF, Argüelles S, Elles S, Ayala A, Oz MF, et al. Lipid Peroxidation: Production, Metabolism, and Signaling Mechanisms of Malondialdehyde and 4-Hydroxy-2-Nonenal. *Oxid Med Cell Longev*. 2014;2014:1–31.
 42. Futschik ME, Carlisle B. Noise-robust soft clustering of gene expression time-course data. *J Bioinform Comput Biol*. 2005;
 43. Martin S, Parton RG. Caveolin, cholesterol, and lipid bodies. *Semin Cell Dev Biol*. 2005;16(2):163–74.
 44. Zumbusch A, Holtom GR, Xie XS. Three-dimensional vibrational imaging by coherent anti-stokes raman scattering. *Phys Rev Lett*. 1999;82(20):4142–5.
 45. Hou J, Williams J, Botvinick EL, Potma EO, Tromberg BJ. Visualization of Breast Cancer Metabolism Using Multimodal Nonlinear Optical Microscopy of Cellular Lipids and Redox State. 2018;(15):2503–13.
 46. Johnson ACM, Stahl A, Zager RA. Triglyceride accumulation in injured renal tubular cells: Alterations in both synthetic and catabolic pathways. *Kidney Int*. 2005;67(6):2196–209.
 47. Ta NL, Seyfried TN. Influence of Serum and Hypoxia on Incorporation of [14C]-d-Glucose or [14C]-l-Glutamine into Lipids and Lactate in Murine Glioblastoma Cells. *Lipids*. 2015;50(12):1167–84.
 48. Yang G, Sau C, Lai W, Cichon J, Li W. Spectral tracing of deuterium for imaging glucose metabolism. 2015;344(6188):1173–8.
 49. Huang KC, Li J, Zhang C, Tan Y, Cheng JX. Multiplex Stimulated Raman Scattering Imaging Cytometry Reveals Lipid-Rich Protrusions in Cancer Cells under Stress Condition. *iScience [Internet]*. 2020;23(3):100953. Available from: <https://doi.org/10.1016/j.isci.2020.100953>
 50. Liberzon A, Subramanian A, Pinchback R, Thorvaldsdóttir H, Tamayo P, Mesirov JP. Molecular

- signatures database (MSigDB) 3.0. Bioinformatics. 2011;27(12):1739–40.
51. Oyadomari S, Mori M. Roles of CHOP/GADD153 in endoplasmic reticulum stress. *Cell Death Differ.* 2004;11(4):381–9.
 52. Bruhat A, Jousse C, Wang XZ, Ron D, Ferrara M, Fafournoux P. Amino acid limitation induces expression of CHOP, a CCAAT/enhancer binding protein-related gene, at both transcriptional and post-transcriptional levels. *J Biol Chem.* 1997;272(28):17588–93.
 53. Pakos-Zebrucka K, Koryga I, Mnich K, Ljubic M, Samali A, Gorman AM. The integrated stress response. *EMBO Rep.* 2016;17(10):1374–95.
 54. Werstuck GH, Lentz SR, Dayal S, Hossain GS, Sood SK, Shi YY, et al. Homocysteine-induced endoplasmic reticulum stress causes dysregulation of the cholesterol and triglyceride biosynthetic pathways. *J Clin Invest.* 2001;107(10):1263–73.
 55. Outinen PA, Sood SK, Pfeifer SI, Pamidi S, Podor TJ, Li J, et al. Homocysteine-induced endoplasmic reticulum stress and growth arrest leads to specific changes in gene expression in human vascular endothelial cells. *Blood.* 1999;94(3):959–67.
 56. Tehlivets O. Homocysteine as a Risk Factor for Atherosclerosis: Is Its Conversion to S-Adenosyl-L-Homocysteine the Key to Deregulated Lipid Metabolism? *J Lipids.* 2011;2011(Figure 1):1–11.

10. FOOTNOTES TO TEXT (IF ANY)

NONE

11. TABLES

TABLE 1

Mean peak height values of phospholipids in methionine media, time-zero samples

<i>lipid species</i> ^a	MB468 mean	MB468 st. dev	MB468resR8 mean	MB468resR8 st. dev	MB468/R8 ratio ^b	<i>p-value</i> ^c
PC	7.5e+07	5.5e+06	7.9e+07	6.1e+06	0.95	3.6e-01
PE	7.3e+06	9.1e+05	2.6e+06	2.7e+05	2.80	1.1e-03
PC/PE	1.0e+01	5.2e-01	3.0e+01	1.2	0.34	5.7e-06
PPC	2.5e+06	3.6e+05	1.2e+05	9.2e+03	20.44	8.6e-04
PPE	3.4e+06	6.1e+05	1.2e+06	1.1e+05	2.94	4.1e-03
PC/PPC	3.0e+01	1.9	6.3e+02	6.4	0.05	4.2e-08
PE/PPE	2.1	1.1e-01	2.2	4.5e-02	0.96	2.0e-01

a. Lipid species were combined for each lipid class within each of the four replicates. These values were then used to calculate the mean values and standard deviations.

b. The MB468 and MB468res-R8 ratios for each lipid class were calculated by taking the MB468 mean value and dividing by the MB468res-R8 (R8) mean value.

c. Significance was calculated using a Welch's t-test (unpaired, two-sided, unequal variance, 95% confidence level) comparing the time-zero, control sample replicate values of MB468 and MB468res-R8.

TABLE 2

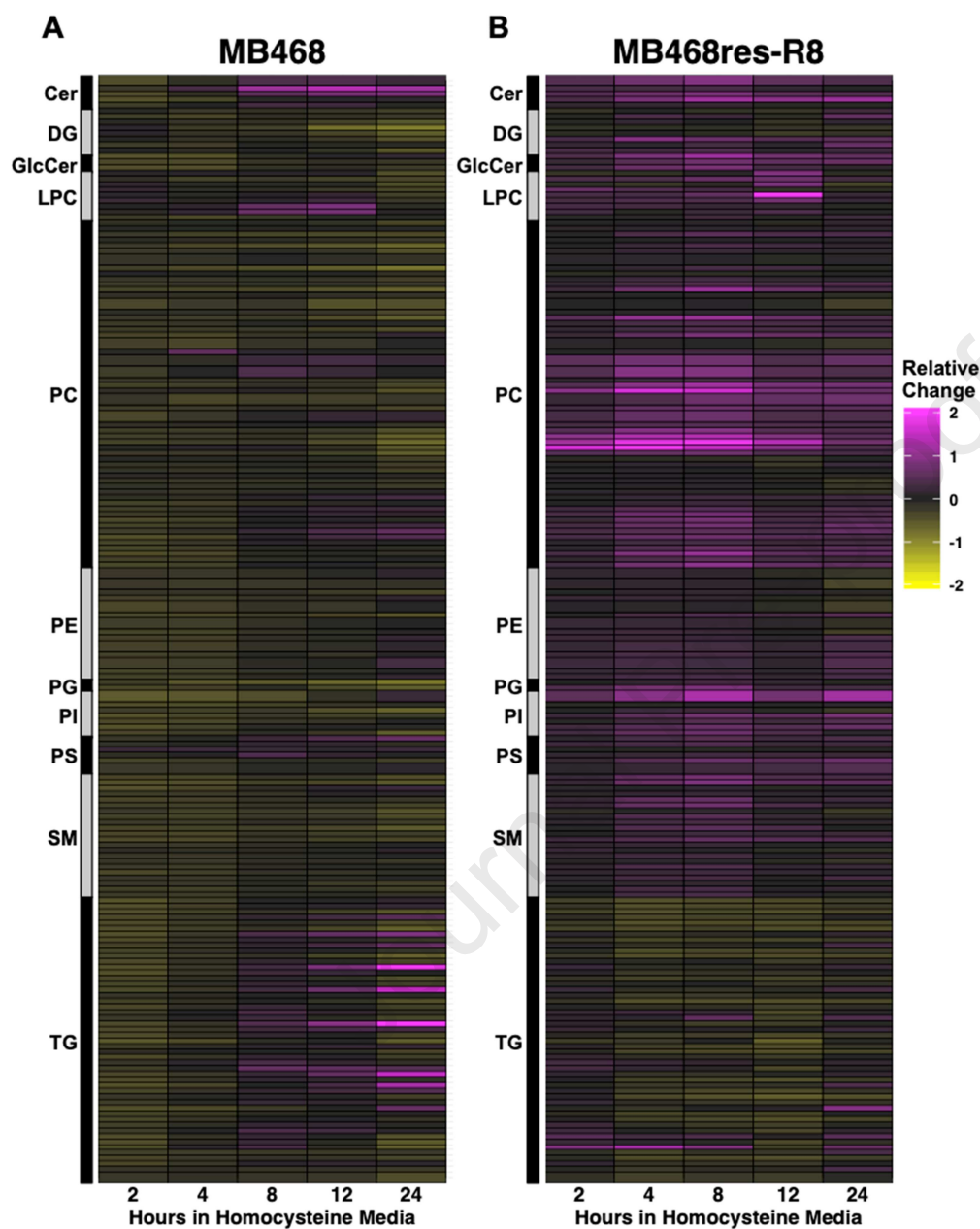
MB468 fatty acid metabolic genes up- or down-regulated at 2 and 12 hours post-media switch as compared to time-zero

<i>GO pathway</i>	<i>Gene^a</i>	<i>Fold Change - 2h</i>	<i>Fold Change - 12h</i>
Biosynthetic Process	PTGIS	0.88	0.19
Biosynthetic Process	FADS1*	0.97	0.22
Biosynthetic Process	MSMO1	0.85	0.22
Biosynthetic Process	EDN2*	0.99	0.23
Biosynthetic Process	FADS2*	0.95	0.24
Biosynthetic Process	PTGS1	0.76	0.24
Biosynthetic Process	SCD	0.89	0.25
Biosynthetic Process	AKR1C3*	1.03	0.26
Biosynthetic Process	FASN*	0.98	0.30
Biosynthetic Process	LTA4H*	1.00	0.37
Biosynthetic Process	ELOVL6*	0.92	0.40
Biosynthetic Process	FA2H*	1.09	0.41
Biosynthetic Process	GGT1	0.65	0.42
Biosynthetic Process	ACLY*	0.97	0.42
Biosynthetic Process	ELOVL5*	1.00	0.43
Biosynthetic Process	ABCD3*	0.93	0.45
Biosynthetic Process	ALOX15*	0.97	0.47
Biosynthetic Process	OXSM*	0.94	2.27
Biosynthetic Process	MGLL*	1.02	2.38
Biosynthetic Process	MLYCD	0.89	2.40
Biosynthetic Process	ALOXE3	2.12	11.43
Beta Oxidation	CRAT*	0.96	0.21
Beta Oxidation	ACADS*	0.90	0.37
Beta Oxidation	ABCD3*	0.93	0.45
Beta Oxidation	ACADM*	1.01	0.48
Beta Oxidation	ECI2	0.89	0.48
Beta Oxidation	BDH2*	1.08	0.49
Beta Oxidation	ACOX3	0.83	0.49
Beta Oxidation	SESN2	4.86	8.10

a. Genes marked with (*) indicate fold change between 0.9 – 1.1 at 2 hours post-media switch

12. FIGURES AND FIGURE LEGENDS

FIGURE 1



Homocysteine media induces a global lipid response in MB468 and MB468res-R8 cells

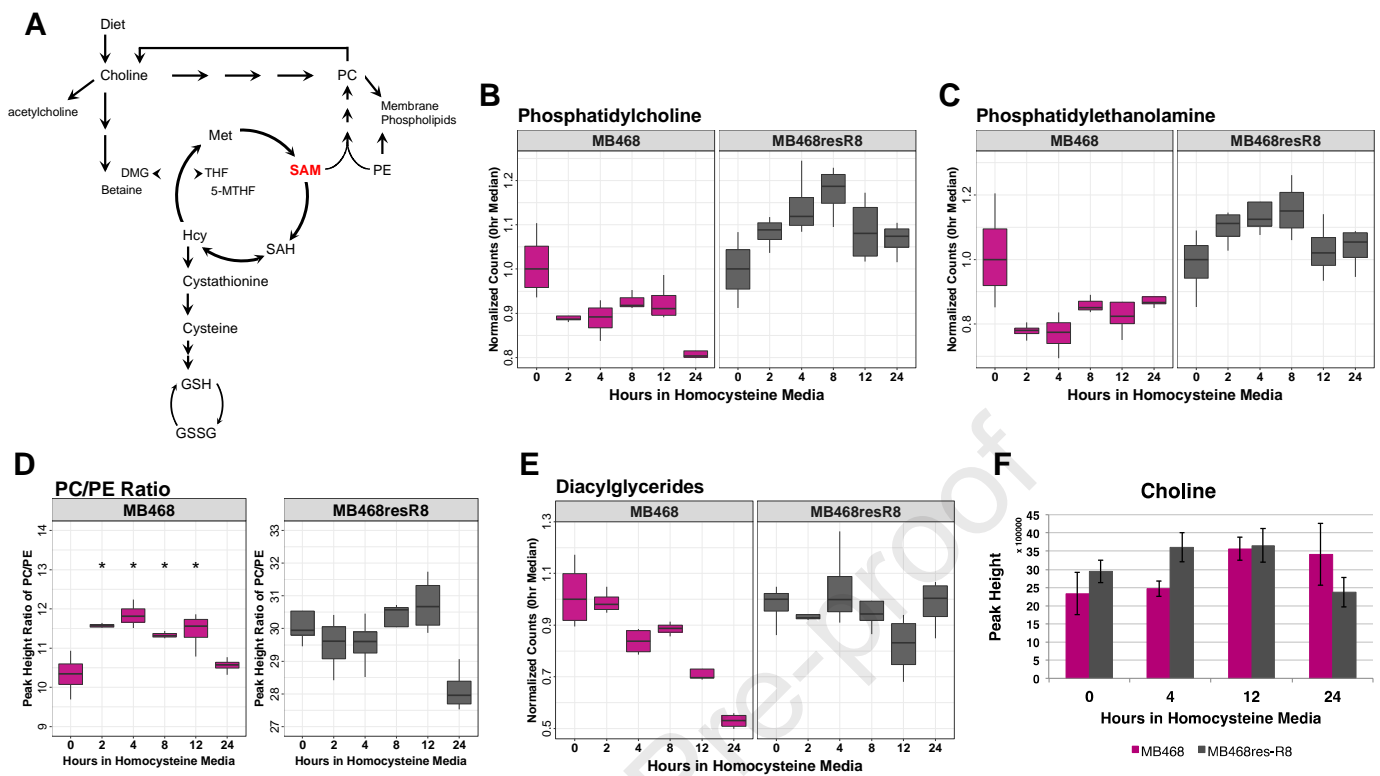
A) MB468 and B) MB468res-R8 cells were cultured in Met⁺ or Met-Hcy⁺ media over the course of 24 hours, measured by UHPLC-QTOF, and normalized to dry cell weight. Heatmaps indicating lipid classes are color filled based on relative change to the Met⁺, time-zero sample. *Yellow* indicates a decrease in metabolite

abundance and *magenta* indicates an increase relative to Met+, time-zero control.

Abbreviations: Cer - ceramide, DG - diglyceride, GlcCer - glucosylceramide, LPC - lysophosphatidylcholine, PC - phosphatidylcholine, PE - phosphatidylethanolamine, PG - phosphatidylglycerol, PI - phosphatidylinositol, PS - phosphatidylserine, SM - sphingomyelin, TG - triglyceride

Journal Pre-proof

FIGURE 2



Phospholipids respond to homocysteine in MB468 cells

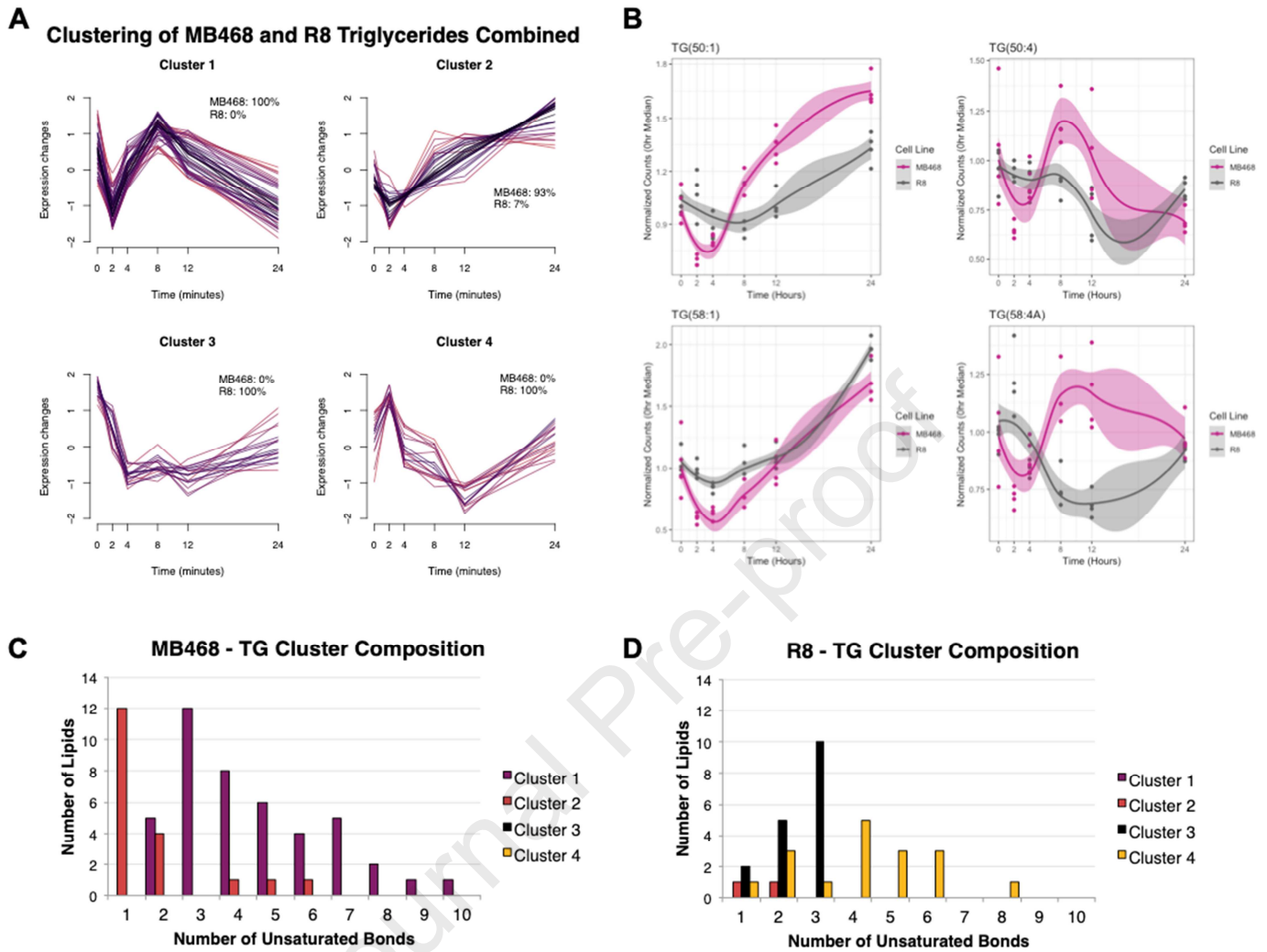
A) Schematic of homocysteine metabolism indicating the connection of SAM and choline in phospholipid synthesis. Three methylation reactions on PE using SAM as a co-factor are necessary to synthesize PC through the PEMT pathway. Choline is used as a precursor to PE in the Kennedy pathway. PC contributes to free choline through the enzyme phospholipase D. Figure adapted from *Obeid et al, 2009 FEBS Letters*. Both MB468 (*magenta*) and MB468res-R8 (*gray*) were cultured in Met⁺ or Met-Hcy⁺ media over the course of 24hrs, measured by UHPLC-QTOF, and normalized to dry cell weight. B) PC and C) PE peak height values of all lipid species within each class were combined for each replicate and plotted for each time point. All time points are normalized to the median value of the Met⁺, time-zero sample. D) The ratio of PC/PE is plotted for MB468 and MB468res-R8 cell lines. Mean values of replicates for A) PC and B) PE were calculated for each time point and PC mean values were divided by PE mean values for each time point. Statistical significance of difference between means was determined by Welch's t-tests and Benjamini-Hochberg procedure using the Met⁺, time-zero sample as a reference, p-values are indicated: * $p \leq .05$. E) Diacylglyceride values were

calculated and plotted as described above for PC and PE. E) Choline peak height values are shown at 0, 4, 12, and 24 hours post-media switch.

Abbreviations: DMG - dimethylglycine, GSH - reduced glutathione, GSSG - oxidized glutathione, Hcy - homocysteine, Met - methionine, 5-MTHF - 5-methyltetrahydrofolate, PC - phosphatidylcholine, PE - phosphatidylethanolamine, PEMT - phosphatidylethanolamine N-methyltransferase, SAH - S-adenohomocysteine, SAM - S-adenosylmethionine, THF – tetrahydrofolate

Journal Pre-proof

FIGURE 3



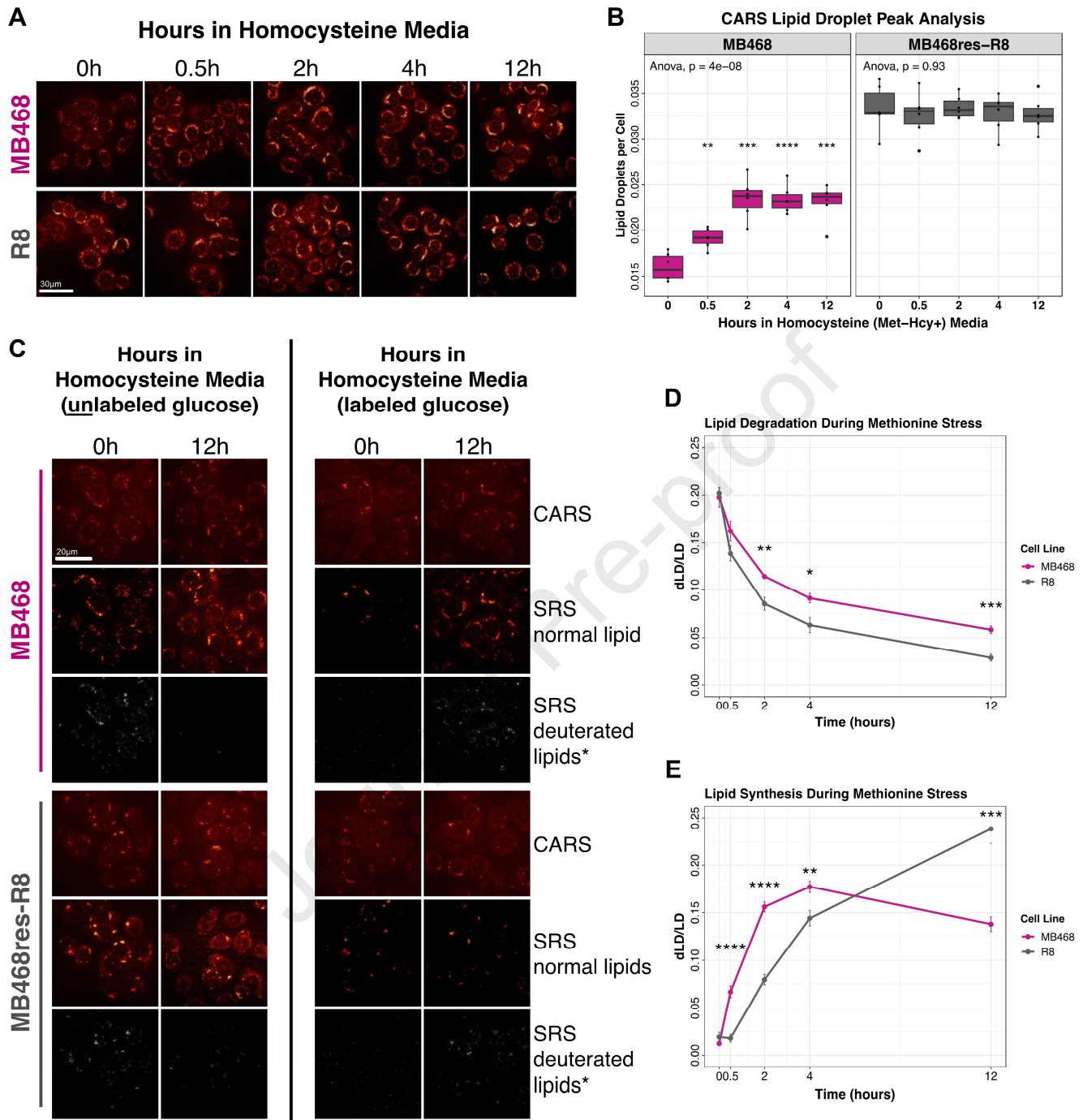
Triglycerides have a distinct response to methionine stress

A) Peak height data for all lipid species in the triglyceride (TG) class were combined for MB468 and MB468res-R8 (R8) cells. For each replicate, mean values were standardized, soft clustered using the R programming software MFuzz, filtered for alpha score values greater than 0.5, and plotted over time (42). The color gradient indicates the strength of the membership value for the cluster (*black* = strong, *magenta* = medium). The percentage of TGs from MB468 and MB468res-R8 (R8) in each cluster are indicated on each plot. B) Representative line plots of MB468 (*magenta*) and MB468res-R8 (*gray*) triglycerides with one or four unsaturated bonds and total tail lengths of 50 or 58 carbons. Confidence level of 0.75 is highlighted in

corresponding line color. C) MB468 and D) MB468res-R8 cells unsaturated TG lipids are plotted for each cluster in A), regardless of total tail length.

Journal Pre-proof

FIGURE 4



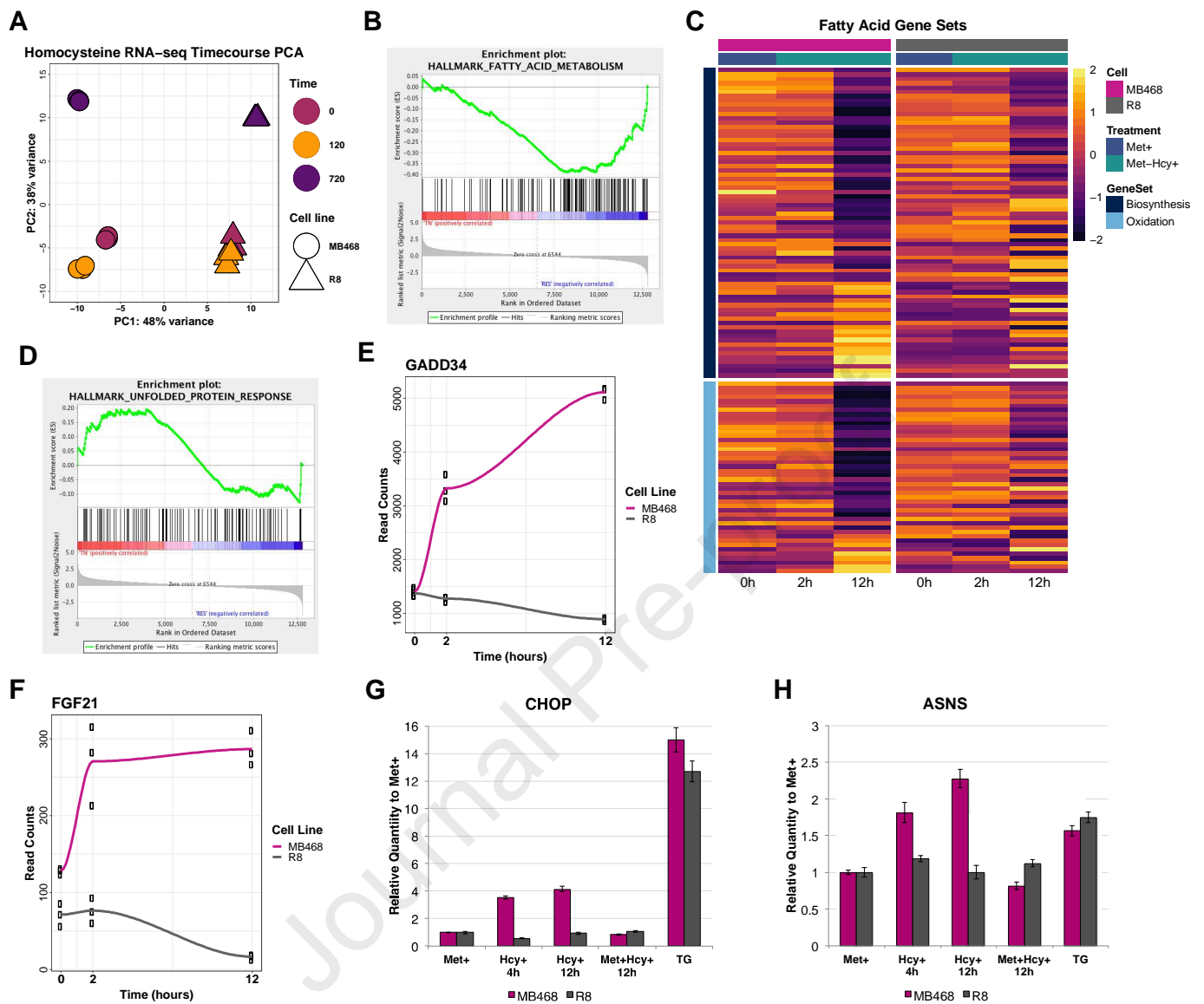
Lipid droplets respond to methionine stress in MB468 cells

A) Representative CARS images of lipid droplets in MB468 and MB468res-R8 cells cultured in Met+ (0h) or Met-Hcy+ (0.5, 2, 4, and 12h) media. The scale bar is 30 μ m. B) MB468 (*magenta*) and MB468res-R8 (*gray*)

samples were plated in duplicate and lipid droplet values per cell from two fields of view per sample are plotted. One-way ANOVA results are reported at the top of each plot. Statistical significance of difference between means was determined by unpaired, two-tailed Student's t-tests and Benjamini-Hochberg procedure using the Met+, time-zero sample as a reference. Adjusted p-values are indicated: ** $p \leq .01$, *** $p \leq .001$, **** $p \leq .0001$. C) Representative CARS (total lipid droplets) and SRS (normal and deuterium-labeled lipids) images of MB468 and MB468-R8 cells at 0h and 12h post-media switch. The scale bar is 20 μm . *Left panel – lipid degradation assay:* MB468 and MB468res-R8 cells were cultured in methionine (Met+) media supplemented with deuterium-labeled glucose for 12 hours followed by a media switch to unlabeled Met+ (0h) or unlabeled Met-Hcy+ (0.5, 2, 4, and 12 hours) media. *Right panel – lipid synthesis assay:* MB468 and MB468res-R8 cells were cultured in unlabeled Met+ media (0h) or labeled homocysteine (Met-Hcy+) media (0.5, 2, 4, and 12 hours). Quantification of SRS deuterium-labeled lipid droplets normalized to SRS total lipid droplets in C) are shown for D) lipid degradation and E) lipid synthesis assays. Statistical significance of difference between means was determined by unpaired, two-tailed Student's t-tests and Benjamini-Hochberg procedure using the Met+, time-zero sample as a reference. Adjusted p-values are indicated: * $p \leq .05$, ** $p \leq .01$, *** $p \leq .001$, **** $p \leq .0001$.

*For visual purposes only, SRS deuterated lipid images are adjusted with an 50% increase in contrast.

FIGURE 5

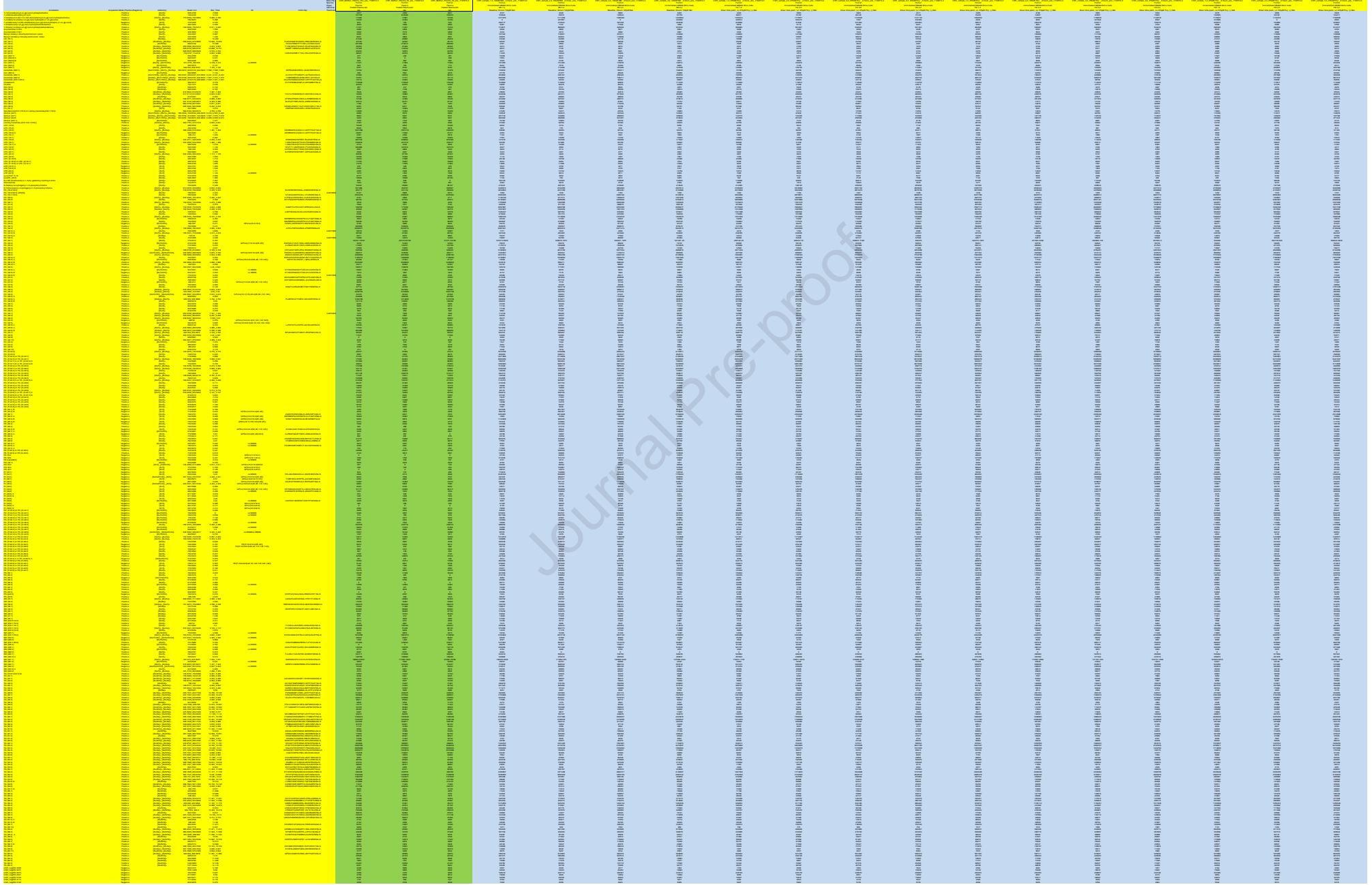


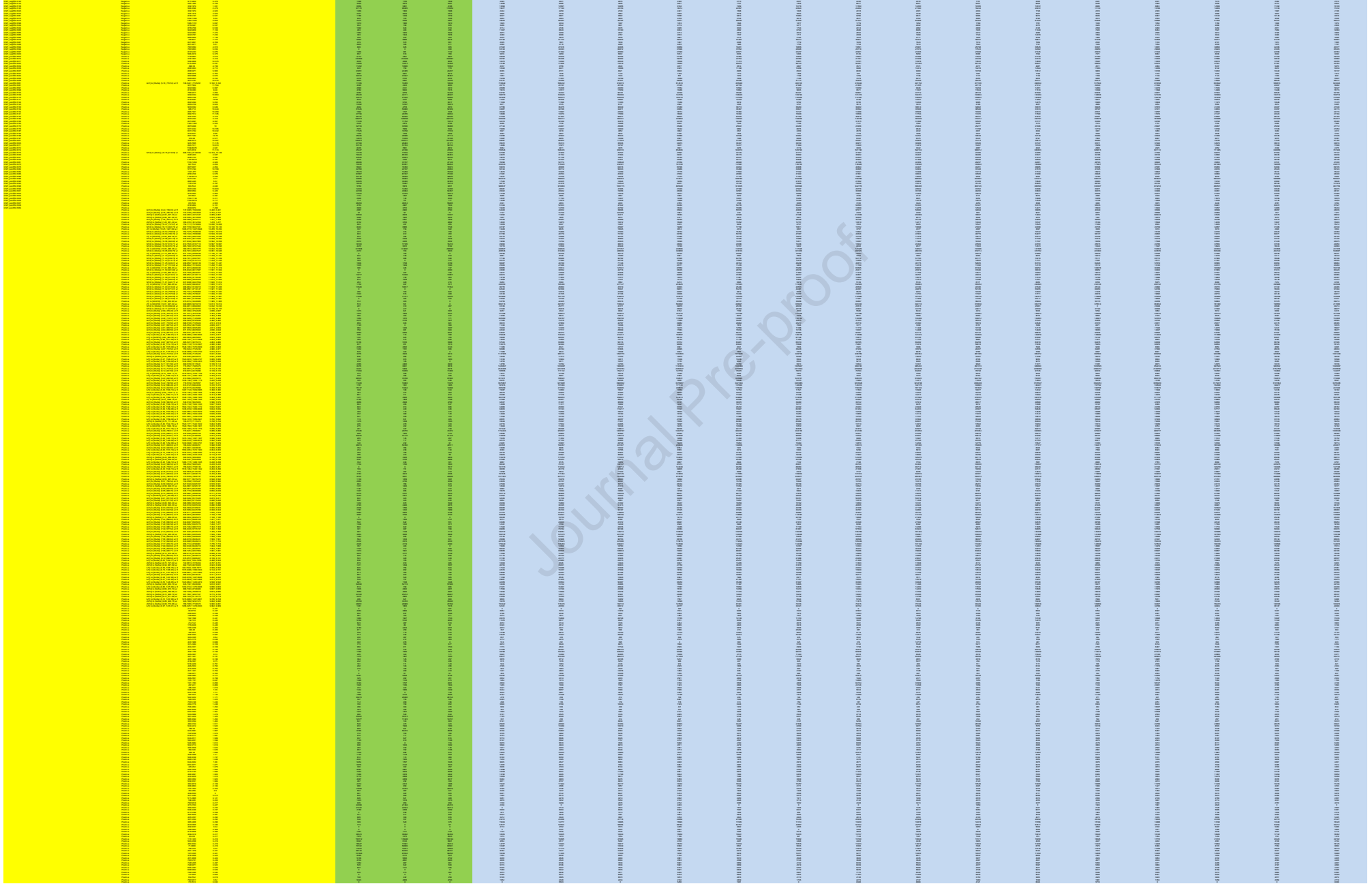
Gene expression during methionine stress

A) MB468 and MB468res-R8 cells were cultured in Met+ (0h) or Met-Hcy+ (2 hr and 12 hr) media and gene expression was analyzed by RNA-seq (single end, 100 bp read length, Illumina HiSeq 4000, n = 3). A principal component analysis (PCA) plot indicates that MB468 (*circle*) and MB468res-R8 (*triangle*) cell lines have distinct genetic profiles but respond in a similar fashion to methionine stress. B) Gene set enrichment analysis (GSEA) of MB468 (*red*) and MB468res-R8 (*blue*) at 12 hours post-media switch indicates a negative correlation between the two cell lines in the fatty acid metabolism gene set. C) Heatmap representing GSEA

gene sets *GO fatty acid biosynthetic process* (dark blue) and *GO fatty acid beta oxidation* (light blue). D) GSEA of MB468 (*red*) and MB468res-R8 (*blue*) at 12 hours post-media switch indicating a mixed response of genes in the unfolded protein response pathway. RNA-seq read counts for E) GADD34 and F) FGF21 in MB468 (*magenta*) and MB468res-R8 (*gray*), which are down-stream targets of the UPR. Quantitative PCR results showing relative expression to Met+, control sample in MB468 (*magenta*) and MB468res-R8 (*gray*) for G) C/EBP homologous protein (CHOP) and H) Asparagine Synthetase (ASNS). Cells were cultured in Met+ (12h), Met-Hcy+ (4, 12h), Met+Hcy+ (12h), or Met+/1uM Thapsigargin (TG, 4h).

Journal Pre-proof





Journal Pre-proof

Journal Pre-proof

Journal Pre-proof

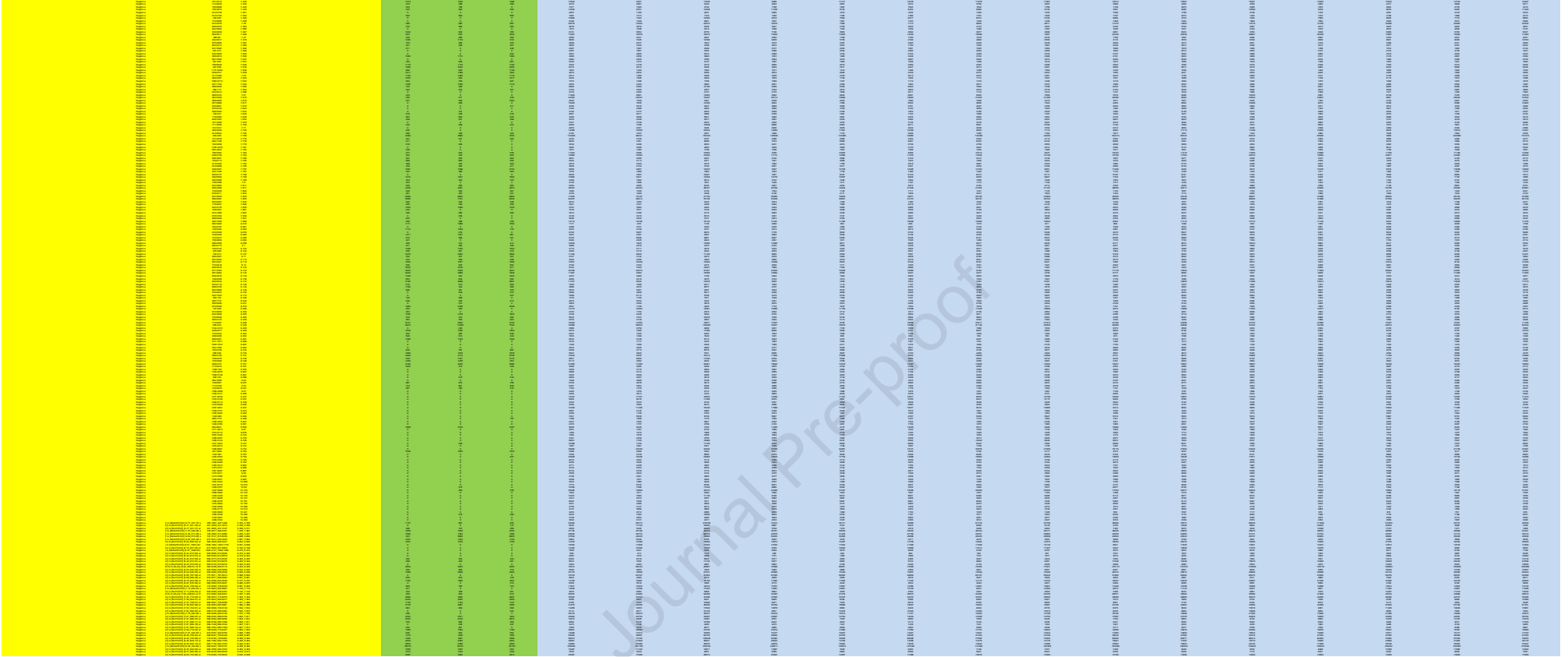
Journal Pre-proof

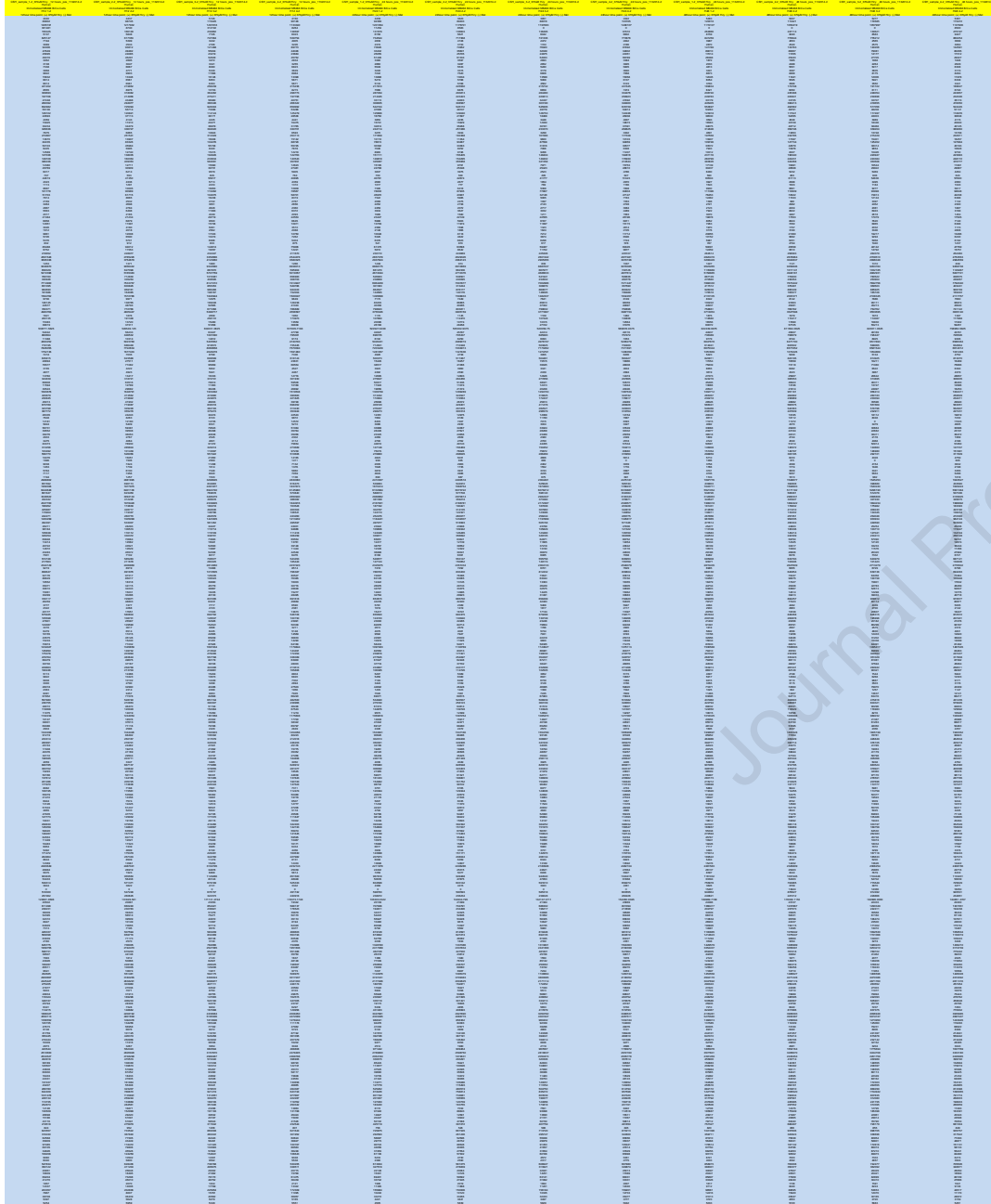
Journal Pre-proof

Journal Pre-proof

Journal Pre-proof

Journal Pre-proof





Journal Pre-proof

Journal Pre-proof

[REDACTED]

Journal Pre-proof

[Redacted content]

Journal Pre-proof

[Redacted content]

Journal Pre-proof

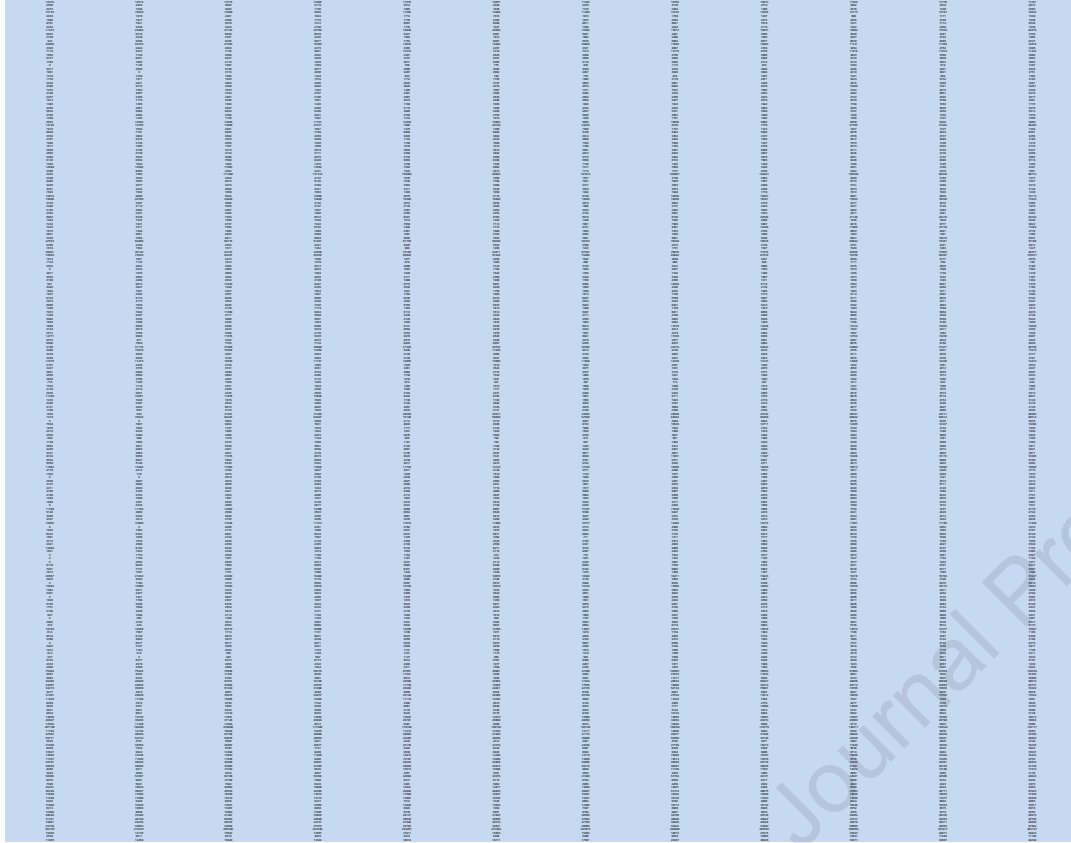
Journal Pre-proof

Journal Pre-proof

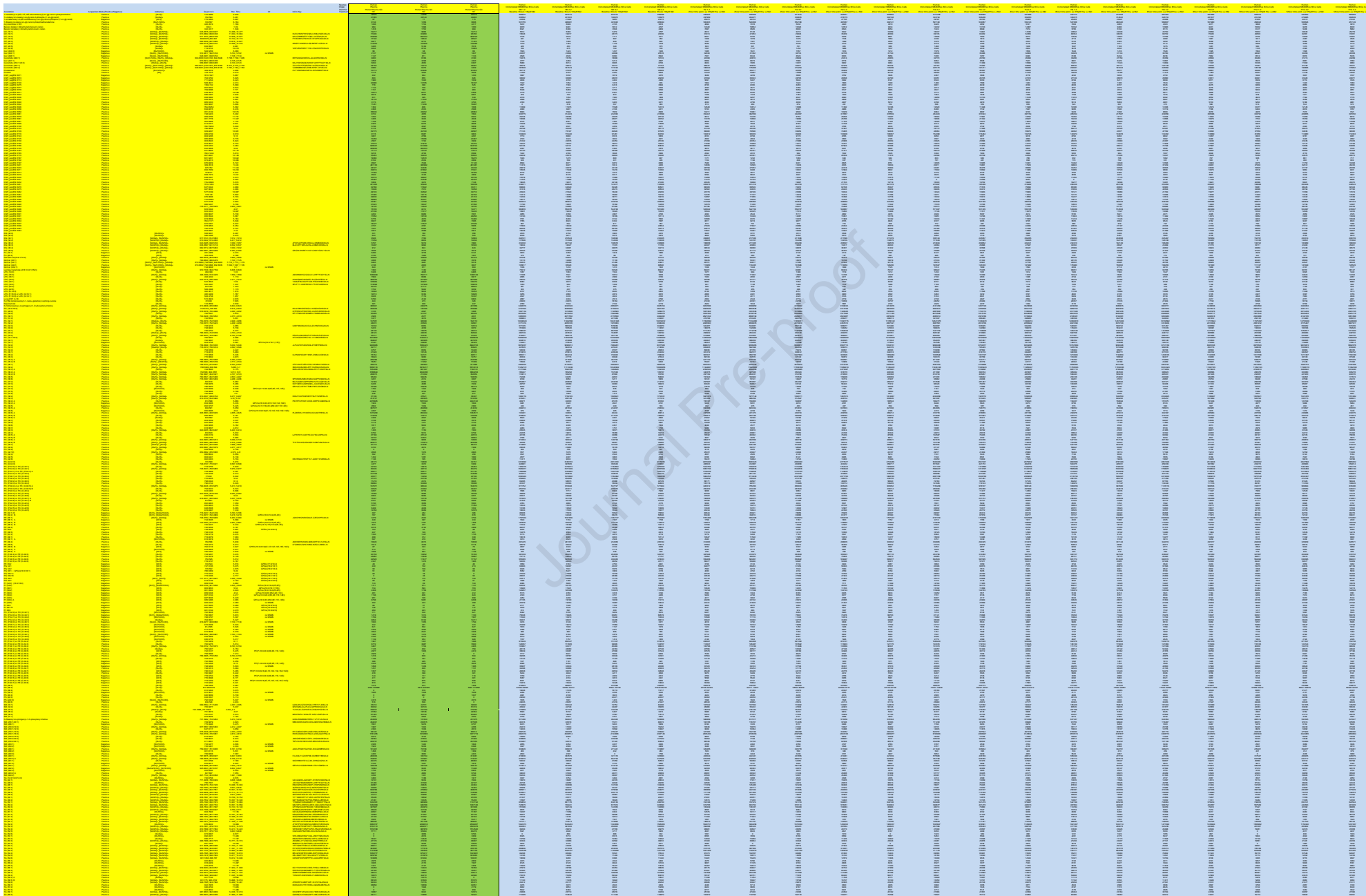
Journal Pre-proof

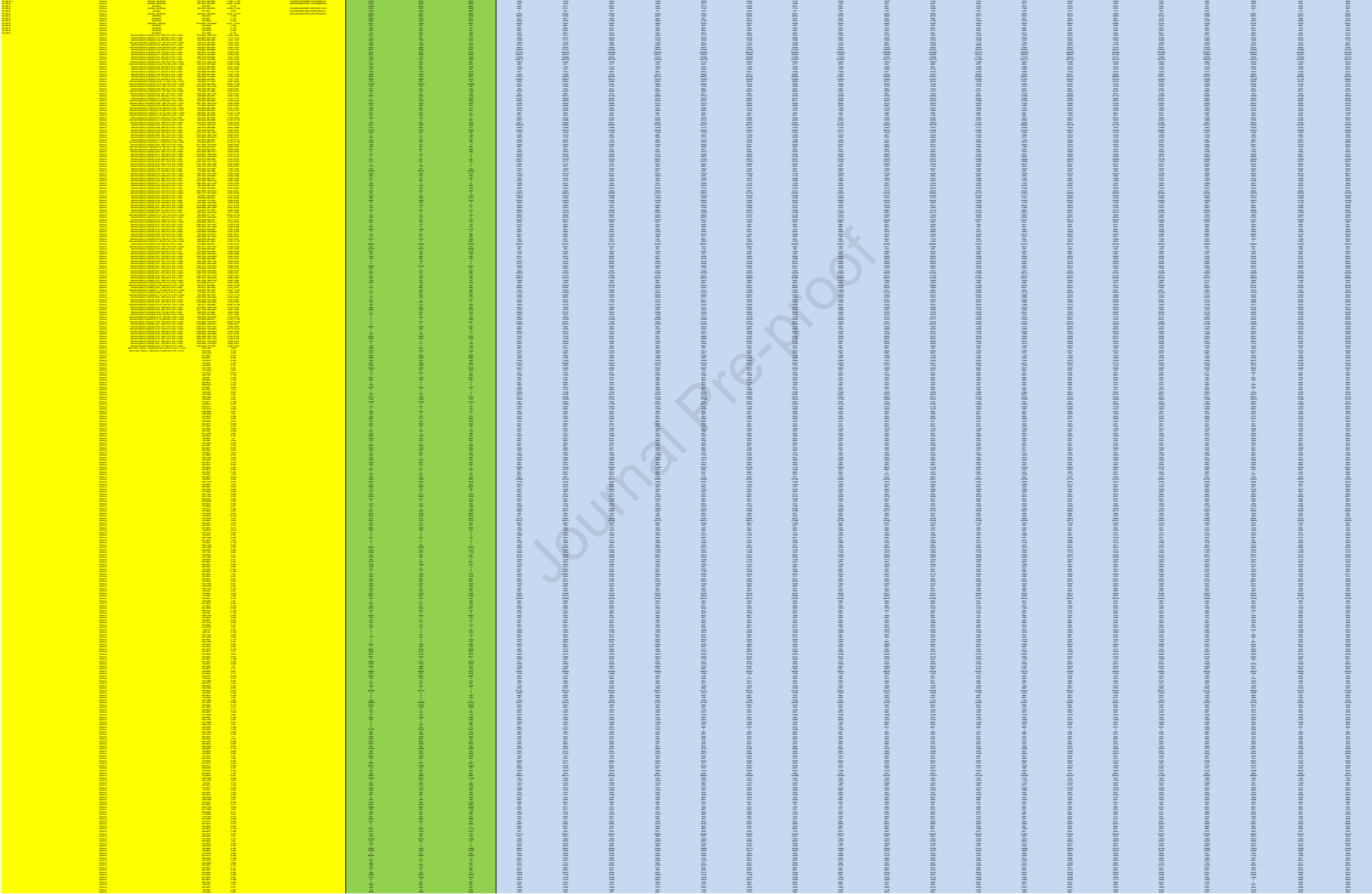
Journal Pre-proof

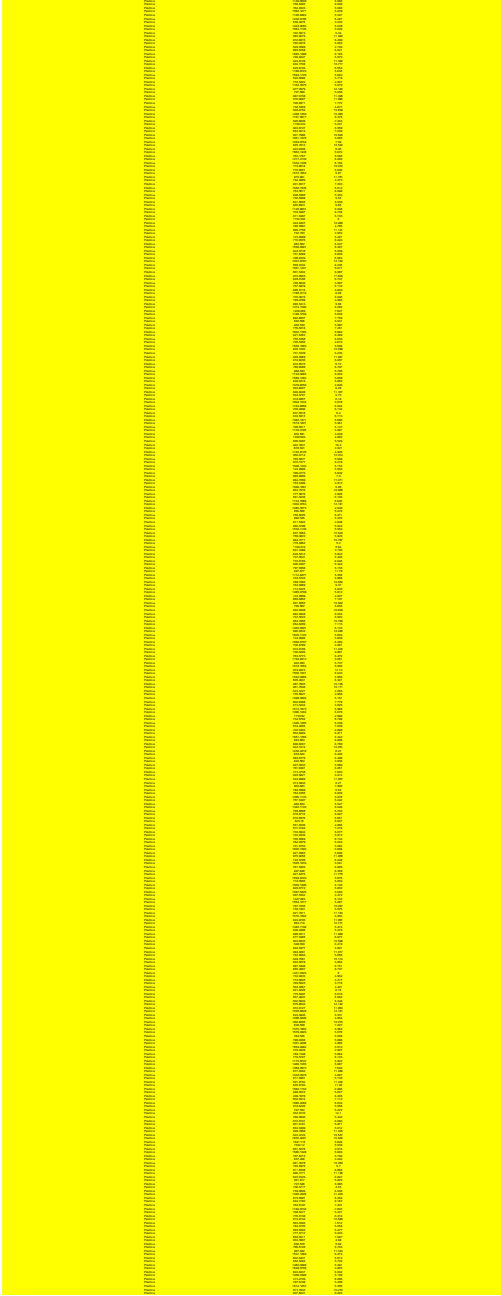
Journal Pre-proof



Journal Pre-proof







Journal Pre-proof

Journal Pre-proof

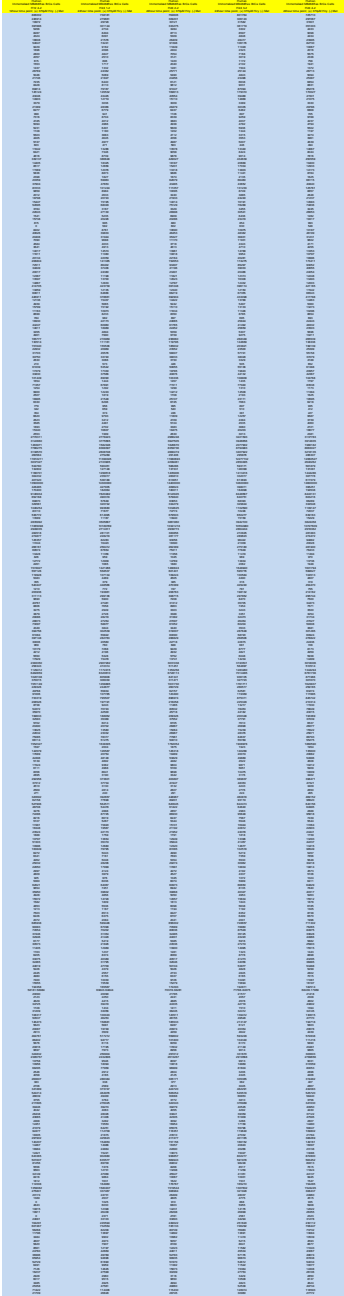


1 1 1

Journal Pre-proof



Journal Pre-proof



Journal Pre-proof

Journal Pre-proof

Journal Pre-proof

Journal Pre-proof

Journal Pre-proof

Journal Pre-proof

Journal Pre-proof



Journal Pre-proof

Mean peak height values of phospholipids in methionine media, time-zero samples

<i>lipid species</i> ^a	MB468 mean	MB468 st. dev	MB468resR8 mean	MB468resR8 st. dev	MB468/R8 ratio ^b	<i>p-value</i> ^c
PC	7.5e+07	5.5e+06	7.9e+07	6.1e+06	0.95	3.6e-01
PE	7.3e+06	9.1e+05	2.6e+06	2.7e+05	2.80	1.1e-03
PC/PE	1.0e+01	5.2e-01	3.0e+01	1.2	0.34	5.7e-06
PPC	2.5e+06	3.6e+05	1.2e+05	9.2e+03	20.44	8.6e-04
PPE	3.4e+06	6.1e+05	1.2e+06	1.1e+05	2.94	4.1e-03
PC/PPC	3.0e+01	1.9	6.3e+02	6.4	0.05	4.2e-08
PE/PPE	2.1	1.1e-01	2.2	4.5e-02	0.96	2.0e-01

a. Lipid species were combined for each lipid class within each of the four replicates. These values were then used to calculate the mean values and standard deviations.

b. The MB468 and MB468res-R8 ratios for each lipid class were calculated by taking the the MB468 mean value and dividing by the MB468res-R8 (R8)\mean value.

c. Significance was calculated using a Welch's t-test (unpaired, two-sided, unequal variance, 95% confidence level) comparing the time-zero, control sample replicate values of MB468 and MB468res-R8.

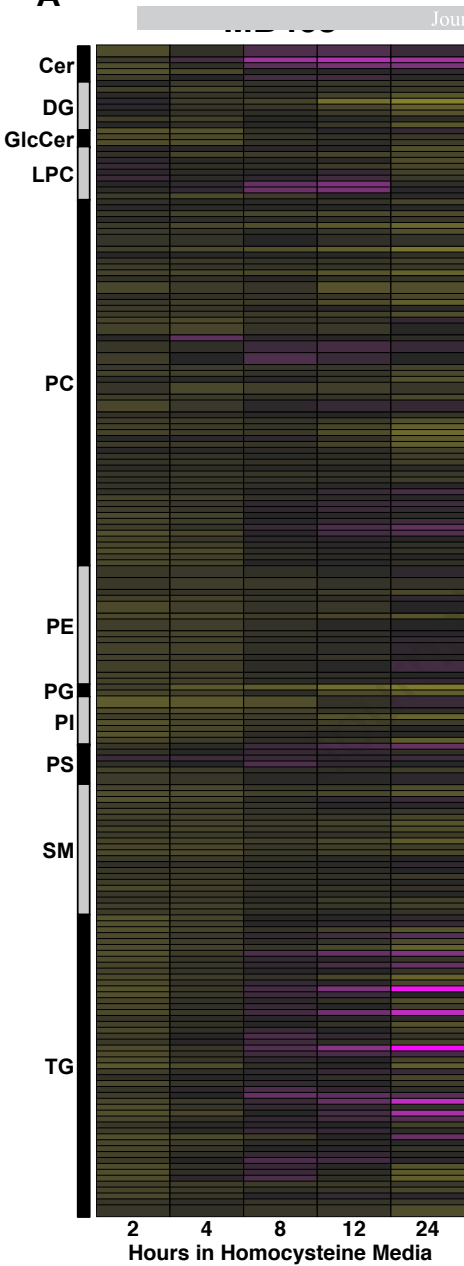
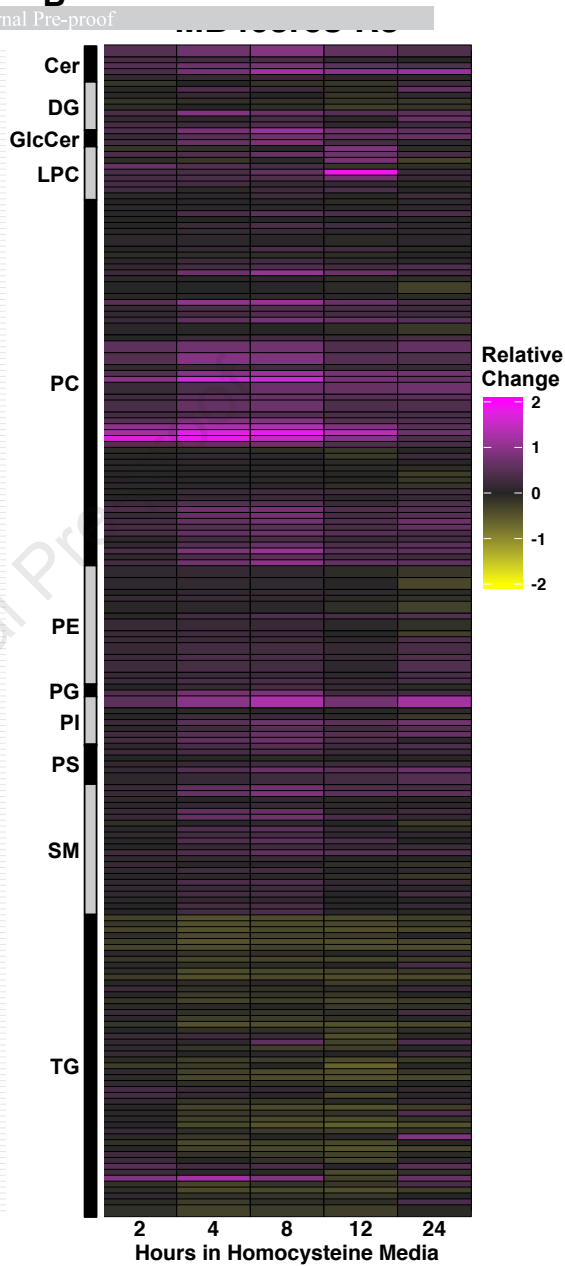
MB468 fatty acid metabolic genes up- or down-regulated at 2 and 12 hours post-media switch as compared to time-zero

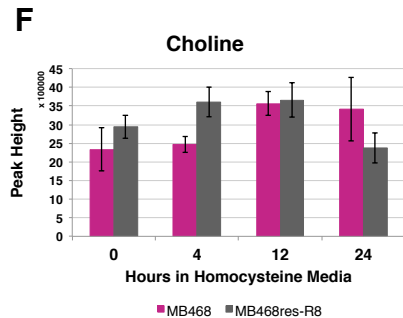
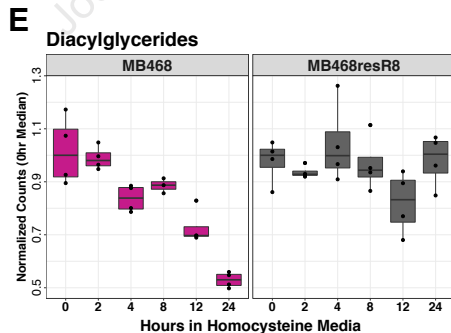
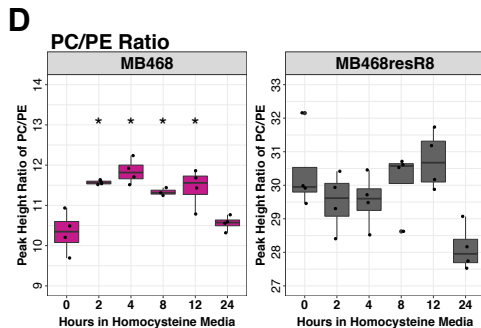
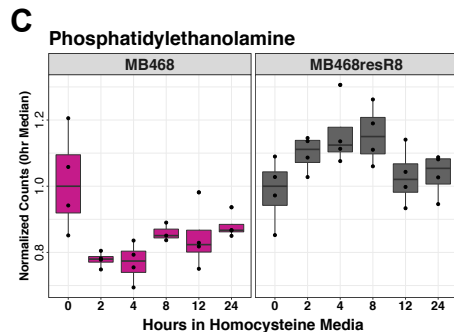
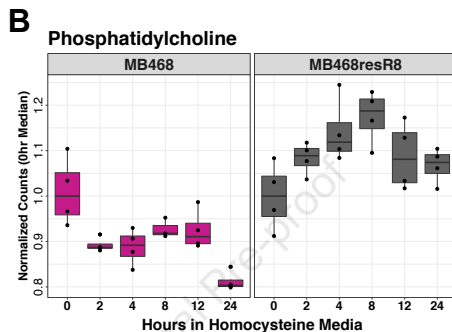
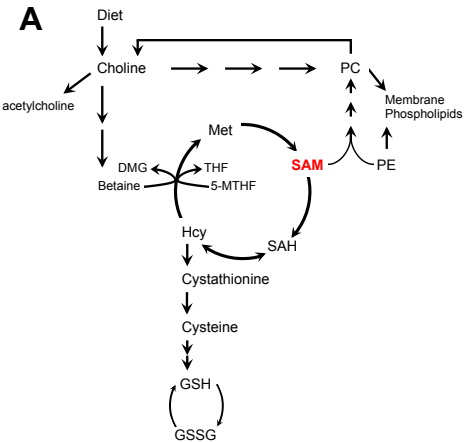
<i>GO pathway</i>	<i>Gene^a</i>	<i>Fold Change - 2h</i>	<i>Fold Change - 12h</i>
Biosynthetic Process	PTGIS	0.88	0.19
Biosynthetic Process	FADS1*	0.97	0.22
Biosynthetic Process	MSMO1	0.85	0.22
Biosynthetic Process	EDN2*	0.99	0.23
Biosynthetic Process	FADS2*	0.95	0.24
Biosynthetic Process	PTGS1	0.76	0.24
Biosynthetic Process	SCD	0.89	0.25
Biosynthetic Process	AKR1C3*	1.03	0.26
Biosynthetic Process	FASN*	0.98	0.30
Biosynthetic Process	LTA4H*	1.00	0.37
Biosynthetic Process	ELOVL6*	0.92	0.40
Biosynthetic Process	FA2H*	1.09	0.41
Biosynthetic Process	GGT1	0.65	0.42
Biosynthetic Process	ACLY*	0.97	0.42
Biosynthetic Process	ELOVL5*	1.00	0.43
Biosynthetic Process	ABCD3*	0.93	0.45
Biosynthetic Process	ALOX15*	0.97	0.47
Biosynthetic Process	OXSM*	0.94	2.27
Biosynthetic Process	MGLL*	1.02	2.38
Biosynthetic Process	MLYCD	0.89	2.40
Biosynthetic Process	ALOXE3	2.12	11.43
Beta Oxidation	CRAT*	0.96	0.21
Beta Oxidation	ACADS*	0.90	0.37
Beta Oxidation	ABCD3*	0.93	0.45
Beta Oxidation	ACADM*	1.01	0.48
Beta Oxidation	ECI2	0.89	0.48
Beta Oxidation	BDH2*	1.08	0.49
Beta Oxidation	ACOX3	0.83	0.49
Beta Oxidation	SESN2	4.86	8.10

a. Genes marked with (*) indicate fold change between 0.9 – 1.1 at 2 hours post-media switch.

<i>lipid species</i> ^a	MB468 <i>mean</i>	MB468 <i>st. dev</i>	MB468resR8 <i>mean</i>	MB468resR8 <i>st. dev</i>	MB468/R8 <i>ratio</i> ^b	<i>p-value</i> ^c
PC	7.5e+07	5.5e+06	7.9e+07	6.1e+06	0.95	3.6e-01
PE	7.3e+06	9.1e+05	2.6e+06	2.7e+05	2.80	1.1e-03
PC/PE	1.0e+01	5.2e-01	3.0e+01	1.2	0.34	5.7e-06
PPC	2.5e+06	3.6e+05	1.2e+05	9.2e+03	20.44	8.6e-04
PPE	3.4e+06	6.1e+05	1.2e+06	1.1e+05	2.94	4.1e-03
PC/PPC	3.0e+01	1.9	6.3e+02	6.4	0.05	4.2e-08
PE/PPE	2.1	1.1e-01	2.2	4.5e-02	0.96	2.0e-01

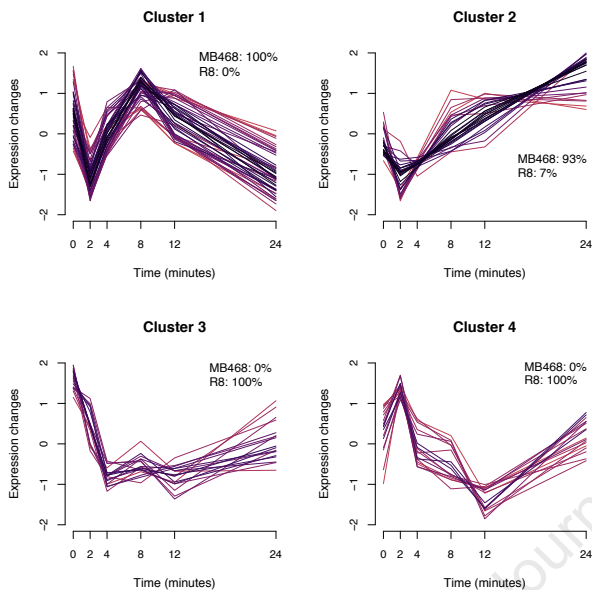
<i>GO pathway</i>	<i>Gene^a</i>	<i>Fold Change - 2h</i>	<i>Fold Change - 12h</i>
Biosynthetic Process	PTGS1	0.68	0.19
Biosynthetic Process	FADS1*	0.97	0.22
Biosynthetic Process	MSMO1	0.85	0.22
Biosynthetic Process	EDN2*	0.99	0.23
Biosynthetic Process	FADS2*	0.95	0.24
Biosynthetic Process	PTGS1	0.76	0.24
Biosynthetic Process	SCD	0.89	0.25
Biosynthetic Process	AKR1C3*	1.03	0.26
Biosynthetic Process	FASN*	0.98	0.30
Biosynthetic Process	LTA4H*	1.00	0.37
Biosynthetic Process	ELOVL6*	0.92	0.40
Biosynthetic Process	FA2H*	1.09	0.41
Biosynthetic Process	GGT1	0.65	0.42
Biosynthetic Process	ACLY*	0.97	0.42
Biosynthetic Process	ELOVL5*	1.00	0.43
Biosynthetic Process	ABCD3*	0.93	0.45
Biosynthetic Process	ALOX15*	0.97	0.47
Biosynthetic Process	OXSM*	0.94	2.27
Biosynthetic Process	MGLL*	1.02	2.38
Biosynthetic Process	MLYCD	0.89	2.40
Biosynthetic Process	ALOXE3	2.12	11.43
Beta Oxidation	CRAT*	0.96	0.21
Beta Oxidation	ACADS*	0.90	0.37
Beta Oxidation	ABCD3*	0.93	0.45
Beta Oxidation	ACADM*	1.01	0.48
Beta Oxidation	ECI2	0.89	0.48
Beta Oxidation	BDH2*	1.08	0.49
Beta Oxidation	ACOX3	0.83	0.49
Beta Oxidation	SESN2	4.86	8.10

A**B**



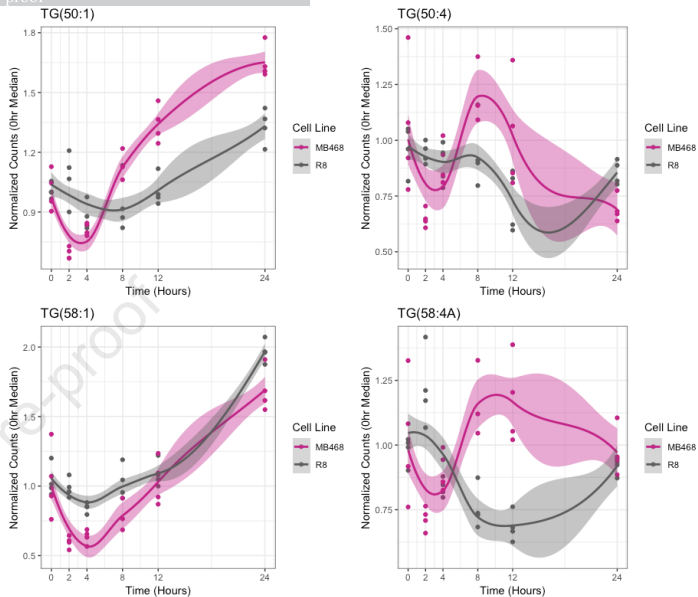
A

Clustering of MB468 and R8



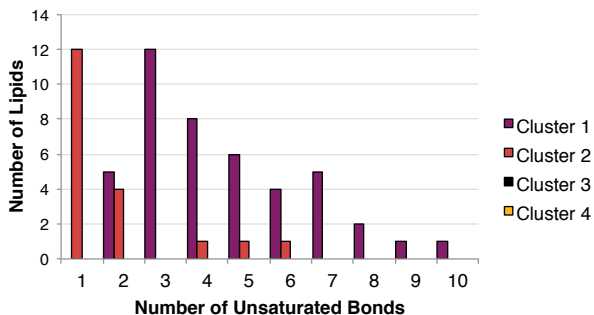
B

Journal Pre-proof



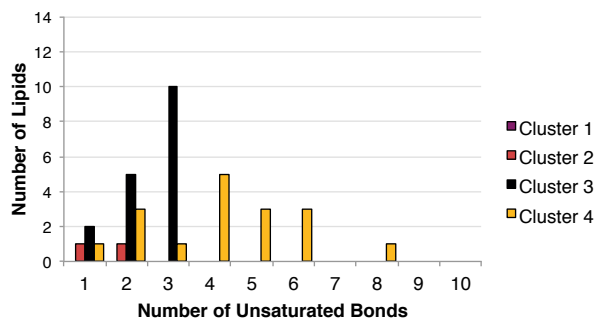
C

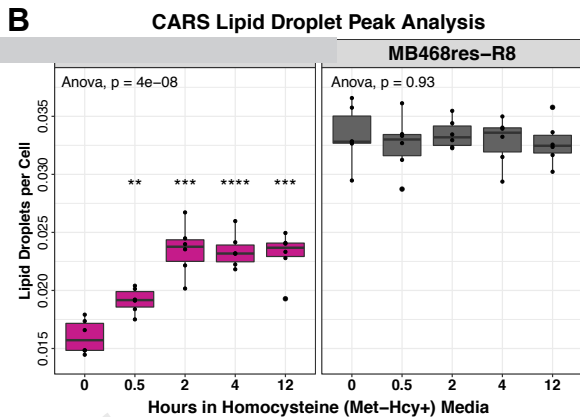
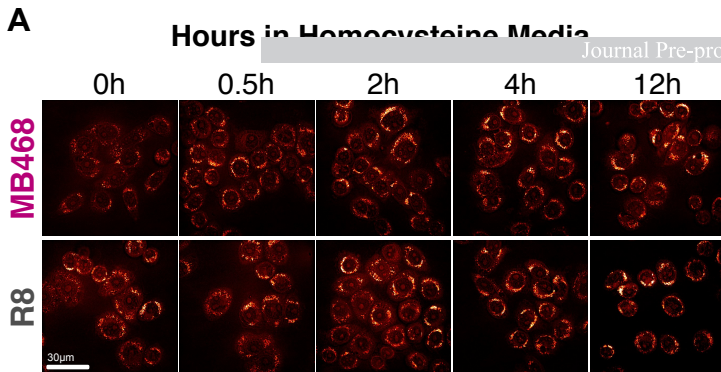
MB468 - TG Cluster Composition



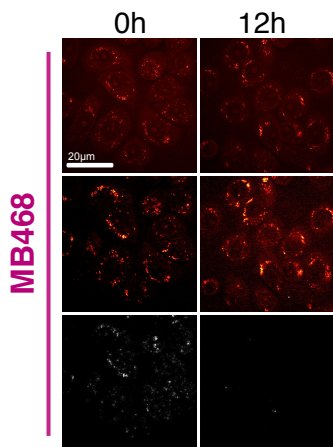
D

R8 - TG Cluster Composition

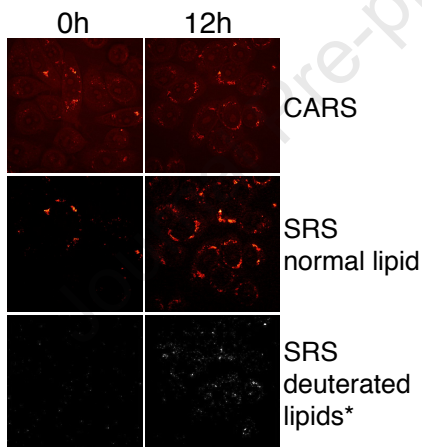




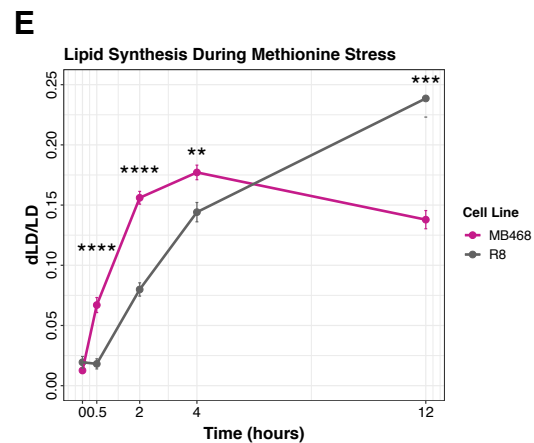
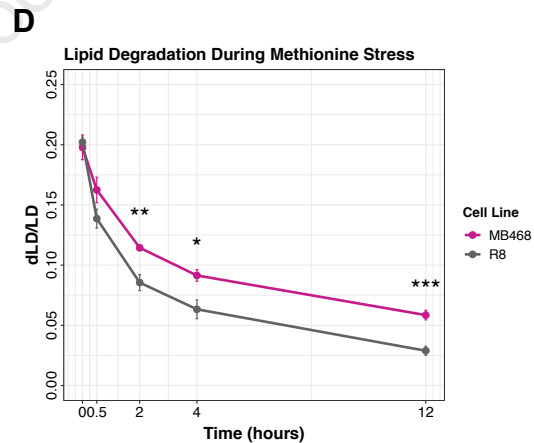
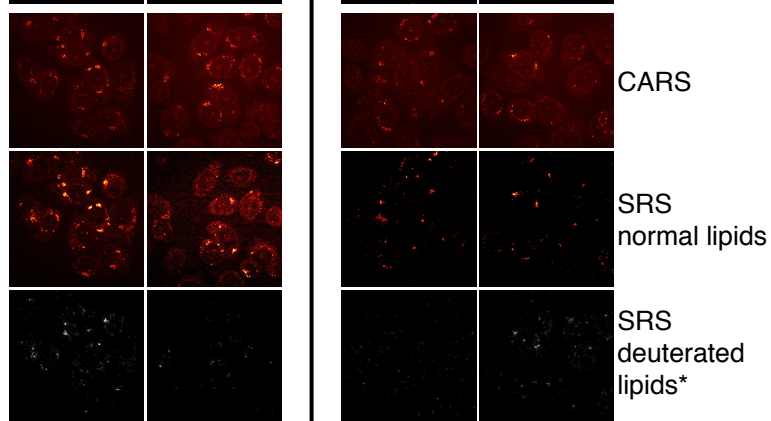
C Hours in Homocysteine Media (unlabeled glucose)

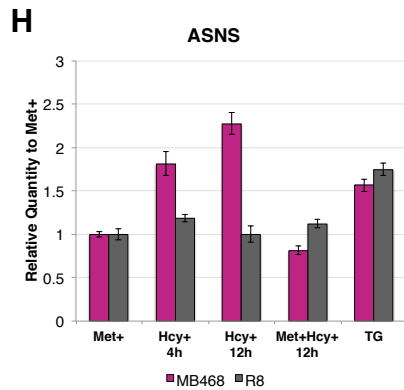
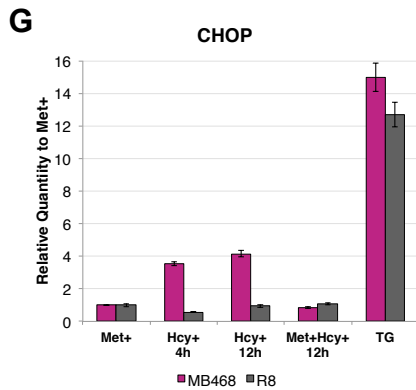
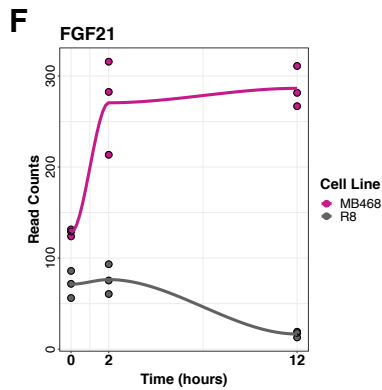
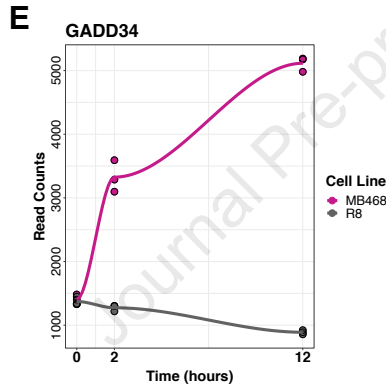
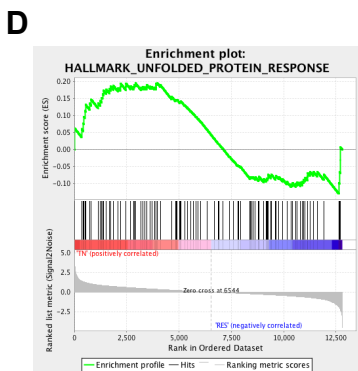
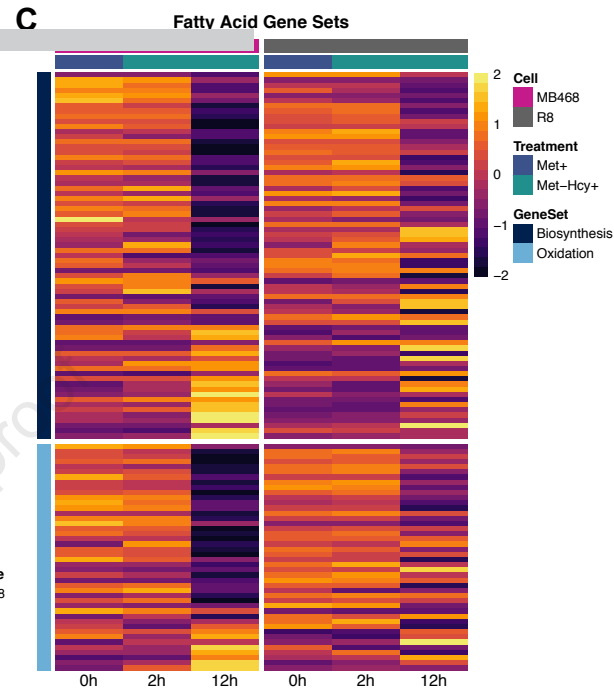
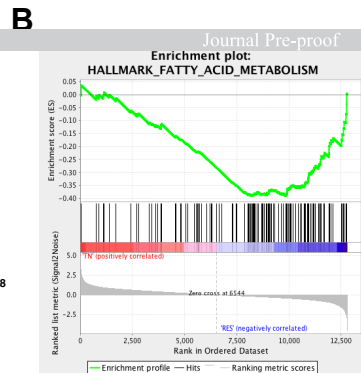
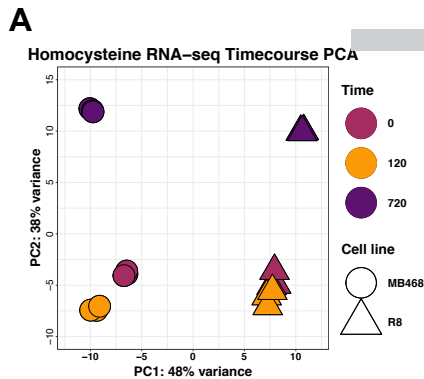


Hours in Homocysteine Media (labeled glucose)



MB468res-R8





**Lipid remodeling in response to methionine stress in MDA-MBA-468
triple-negative breast cancer cells**

Stacey L. Borrego ¹, Johannes Fahrman ^{2,3}, Jue Hou ⁴, Da-Wei Lin ¹,

Bruce J. Tromberg ^{4,5}, Oliver Fiehn ², Peter Kaiser ¹

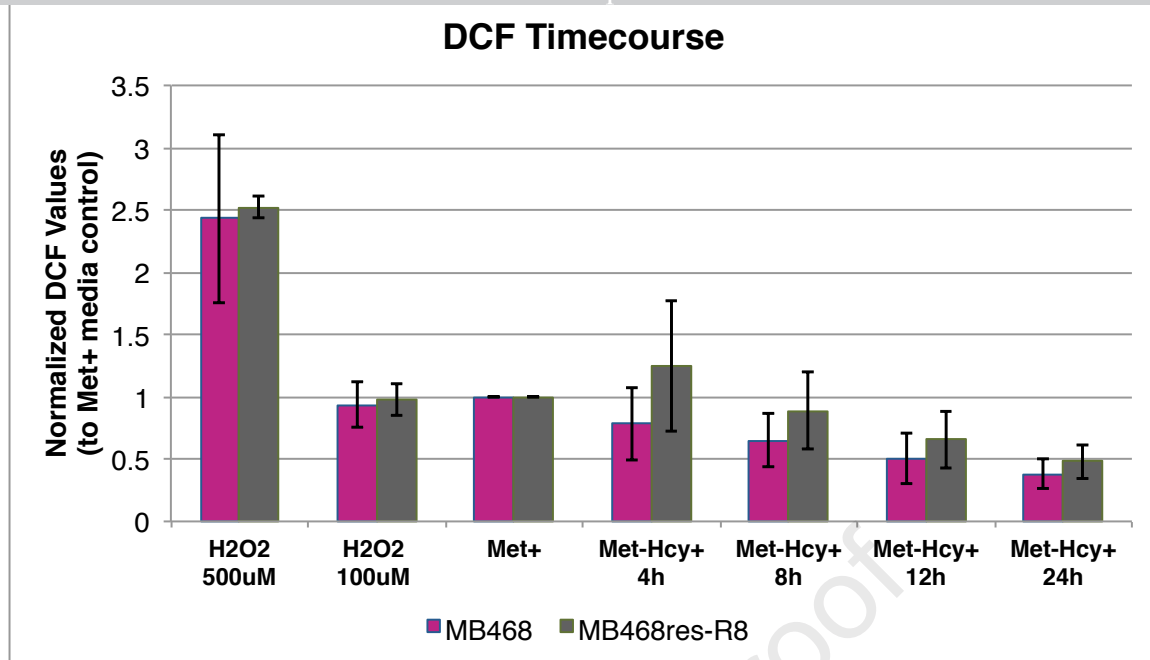
1 – Department of Biological Chemistry, University of California, Irvine, Irvine, CA

2 – West Coast Metabolomics Center, University of California, Davis, Davis, CA

3 – Department of Clinical Cancer Prevention, University of Texas MD Anderson Cancer Center,
Houston, TX

4 – Department of Biomedical Engineering, University of California, Irvine, Irvine, CA

5 – National Institute of Biomedical Imaging and Bioengineering, Bethesda, MD



Supplemental Figure S1: Measure of reactive oxygen species in MB468 and MB468re-R8 cells

ROS levels were assessed by flow cytometry using the general oxidative stress indicator chloromethyl-H2DCFDA (Invitrogen, C6827) per manufacturer's instructions. Cells were cultured with hydrogen peroxide (H_2O_2) as positive controls, Met+ media as experimental control, and Met-Hcy+ media. The data represented are the medians of 3 experiments normalized to the median of Met+ control sample +/- standard deviation.